THEORETICAL INVESTIGATION OF THE STRUCTURE AND FUNCTION OF MAO IN ACTIVATION OF METALLOCENE OLEFIN POLYMERIZATION

Muhammad Sajid Iqbal

Abstract

Olefin polymerization by single a site metallocene catalyst is an intensive research area since last decade. Metallocene pre-catalysts are capable to provide a good control of polymer microstructure, molecular weight and stereospecificity. Higher catalytic activity of metallocenes are achieved by using methylaluminoxan (MAO) co-catalyst but up to now MAO structure is still illusive. Many theoretical MAO structures were purposed to understand the pre-catalyst activation mechanism however none of structure is generally accepted. In this study, MAOs affinity for chloride/methyl ligands to form respective MAO anions relative to chloride/methyl trimethylaluminum anions is addressed. MP2 level of calculations were performed for the formation of MAO-Cl^-/Me^- anions. Tetra-coordinated Al- sites were identified in agreement with the experimental and theoretical results. TMA contents at various concentrations were investigated and results showed that TMA deficient MAO models have higher affinities than fully saturated MAOs. Hexagonal rings were formed by the most stable anions and their affinity is directly influenced variation in composition. The results suggested the hexagonal rings in combination with square rings might be considered as part of real MAO. Structural isomerism among MAOs significantly affects the ligand affinities. Later on, the electrostatic potential maps confirm the higher stability of MAO anions than TMA anions which is corresponded to higher catalytic affinity of metallocene.

Furthermore Cp_2ZrCl_2/MAO interaction was studied by using different DFT functions to assess the performance of DFT functions as compared to MP2 calculations. It was concluded that M062X and WB97XD methods provide results in good agreement with the MP2/TZVP ones, and hence these functionals represent promising DFT methods for future studies.

Contents

Abbreviations & Notations

BE	Binding energy
DFT	Density functional theory
DMAH	Dimethylaluminum hydroxide
DPP	Diphenylphenol
DRIFTS	Diffuse reflectance infrared spectroscopy
EAO	Etheylaluminoxane
EPMA	Electron probe microanalysis
ESP	Electrostatic potential surfaces
FTIR	Fourier transform infrared spectroscopy
HAO	Higher alkylaluminoxane
HFIP	Hexafluoropropanol
IBAO	Isobutylaluminoxane
LSDA	Local spin-density approximation
MAO	Methylaluminoxane
MP2	Møller–Plesset perturbation theory of the second order
MS	Mass spectrometry
NMR	Nuclear magnetic resonance
PCP	Pentachlorophenol
PFA	Pentafluoraniline
PFP	Pentafluorophenol
SEM	Scanning electron microscopy
SVP	split valence and polarization
TAAO	Tetraalkylaluminoxane
TFHQ	Tetrafluoroquinone
TMA	Trimethylaluminum
TZVP	triple-zeta valence and polarization

XPS	X-ray photoelectron spectroscopy
ΔE_{Cl^-}	Relative electronic affinity of MAO for chloride ligand
ΔE_{Me^-}	Relative electronic affinity of MAO for methyl ligand

1 General Literature Part

1.1 Introduction

Olefin polymerization by transition metal catalyst dates back to discovery of transition metal halides such as $TiCl_4$, $TiCl_3$, $ZrCl_4$ in combination with aluminum compounds by Ziegler and Natta, [1], [2] who shared a Nobel Prize in 1963 for their work. Ziegler-Natta catalysts were classified into two categories on the base of physical state rather than catalytic mechanism. Heterogeneous $TiCl_3$ catalyst supported on anhydrous $MgCl_2$ surface was found very successful in polymerization because it eliminates the possible steps related to catalyst removal from product and solvent purification. These features not only enhance the catalytic efficiency but also make it economically favorable. Breslow and co-workers [3] exposed homogenous catalyst which did not draw extensive interest for over 20 years because of low catalytic activity, short kinetic life time and deficient in stereospecific control. However, recent homogenous metallocene catalysts including MAO co-catalyst boost the scientific and industrial interest. [4]

Metallocene catalysts used in olefin polymerization, is the most emerging application of organometallic chemistry in industrial development. Titanocene dichloride in combination with aluminum alkyl chlorides were mostly used for ethene polymerization in early days since 1957 with a low catalytic activity, short kinetic life time and lack of stereospecific control. In order to find alternative catalytic precursors to replace $TiCl_2$ catalyst, analogous research was conducted by Breslow and Newburg [3] on zirconocene chloride including alkyl aluminum compounds. There was no significant improvement with these catalysts. However Sinn and Kaminsky [5] discovered that the activating effect was highly increased by small addition of water to zirconocene catalytic system. [6]

Metallocene catalysts are widely used for olefin polymerization and organic synthesis. Zirconocene catalysts are generally used in a combination with alkylaluminium compounds. Monoalkyl zirconocenium cations are considered as active catalysts for olefin polymerization which are generated by the addition of co-catalysts such as borates, boranes or methylaluminoxane (MAO). [7] Discovery of homogeneous single site metallocene catalyst stimulated new research area in olefin polymerization. Metallocene catalyst provides efficient control of stereochemistry of polymers and co-monomer combination while there is need of additional steps to separate metal residue from polymer. Efficiency of metallocene catalysts is further enhanced by using different co-catalysts. [8], [9]

In early days, free-radical initiators, Phillips type catalysts and Ziegler-Natta catalysts were used for polyolefins preparation but nowadays homogeneous catalysts derived from metallocene complexes are mostly used for olefin polymerization due to their stereoselectivity, high activity and the narrow molecular weight distribution. The catalytic system works very slowly in the absence of aluminum compounds, however addition of water to aluminum containing catalysts, enhance the catalytic activity because hydrolysis of aluminum compounds involves the formation of aluminoxane MAO co-catalyst.[10], [11] Chemical functionality of MAO co-catalyst is not well

understood due to deficient structure determination of MAO. In order to understand the nature and chemical mechanism of catalyst, it is necessary to understand the MAO structure. However theoretical studies are being carried out to investigate MAO structure and its functionality. [12]

1.2 Catalyst components

Catalyst components in olefin polymerization are; metallocene, aluminum compounds and solvent systems.

1.2.1 Metallocenes

Metallocenes (LL´MtX$_2$) are transition metals from group four of periodic table with d^0 electronic configuration. L, L´ represents the π ligands while X$_2$ for two σ ligands. Metallocenes exist in different structural form due to change in ligands. Different π substituent ligands are responsible for the change in symmetry. General structure of metallocene is represented in Figure 1 along with plane angles. β and E in Figure 1 represent the bite angle and bridge angles respectively. Bridge angles determine the rigidity of the structure. Different possible structures due to different π ligands are represented in Table 1.
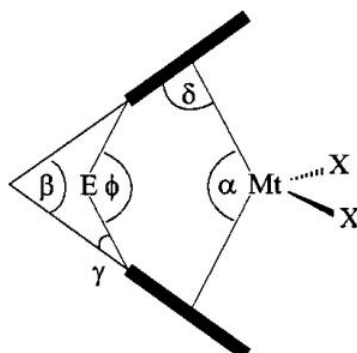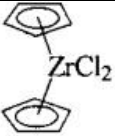

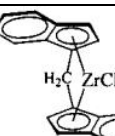*Figure 1. General structure of metallocene* [13]
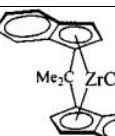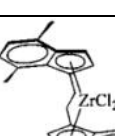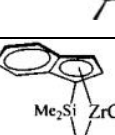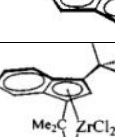
Metallocenes initiator systems were studied intensively rather than traditional Ziegler-Natta initiators because metallocene precursors provide better understanding about iso-selectivity of the products. Many metallocenes accelerate polymerization 100 fold faster than conventional heterogonous catalytic precursors because of homogenous phase, active role of each transition metal atom and formation of variety of polymers. In particular, zirconocenes offer some practical advantages like stability at conventional polymerization temperatures, low relative cost of materials, and high catalytic activities. [13], [14]

1.2.2 Co-catalysts

Cationic palladium complexes [Pd(NCR)$_4$]$^{2+}$2X$^-$ were found to be active without a co-catalyst. However most of metallic complexes require co-catalyst for proper activation essential for olefin

polymerization. Mostly MAO is used as co-catalyst, followed by other alternative co catalysts such as perfluorinated boranes. Methylaluminoxane has shown great capability in formation of active metallocene site by abstracting chloride ligands (σ ligands) and active site is further

Table 1. Zirconocene with respective bond angle [14]

Zirconocene	α	β	Υ	φ	δ
	129,0	53,5			88,8
	116,6	71,4	14,2	99,8	86,0
	117,4	72,4	14,5	101,4	84,8
	118,1	70,9	14,4	99,7	85,0
	126,9	62,1			84,6
	125,3	59,9			85,8
	127,8	61,8	16,3	94,6	84,8
	118,3	75,1	12,5	100,1	83,0

stabilized by the formation of stable MAO counter anion. [11] Yang *et al.* [8] and Ewen *et al.* [9] observed that tris(perfluoroaryl)borane was also capable of activating a catalyst. The perfluorinated boranes were employed alone or along with the combination of aluminoxane. Here some examples of perfluorinated boranes are given used as co-catalyst such as tris(pentafluorophenyl) borane, $B(C_6F_5)_3$ and trityltetrakispentafluorophenyl)borate, $Ph_3C^+B(C_6F_5)_4^-$, boron trifluoride/etherate, $BF_3 \cdot Et_2O$. Nonperfluorinated boranes co-catalyst like triphenylborane $B(C_6H_5)_3$ were also reported. [15]
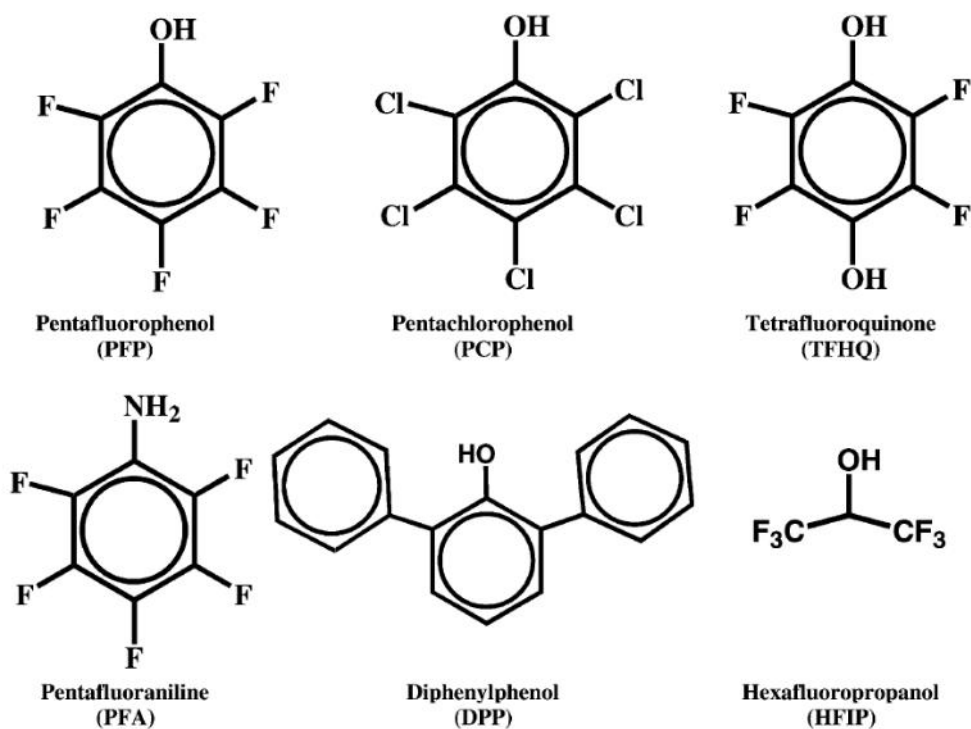

Figure 2. Alternative hetero compounds for modified co-catalyst [11]

Sterically crowded perfluoroarylaluminum derivatives i.e. Al $(C_6F_5)_3$ and $[Ph_3C]^+ [Al(C_6F_5)_4]^-$ also impart effective role in metallocene activation. Trityl salts $[Ph_3C]^+[Al(OC_6F_5)_4]^-$ is an effective co-catalyst for Cp_2ZrMe_2. Different co-catalytic systems were synthesized by treating aluminum compounds with other compounds containing hetero atoms like nitrogen or oxygen. These new modified aluminum alkyl and aluminoxane co-catalysts revealed good co catalytic ability toward metallocene precursors. Figure 2 represent new reacting compounds for preparing alternative co-catalysts. [16], [17], [18]

1.2.3 Solvent/carriers

Aluminoxanes are mostly soluble to aromatic organic compounds. Mostly toluene and benzene solvents are used.

1.3 Polymerization process

Olefin polymerization involves the following steps;

1.3.1 Activation

Metallocene alkyl cation is considered as an active centre in olefin polymerization. Activation proceeds by the reaction of metallocene with co-catalyst which forms a highly reactive cationic metallic centre as given in scheme 1. Methylaluminoxane is used as co-catalyst to activate the catalytic zirconocenes. In the first step, alkylation of metallocene take place in which aluminum atom abstracts one of the halide atoms from zirconocene, while the next step involves the formation of cationic metal centre, acting as activated catalyst. [14]
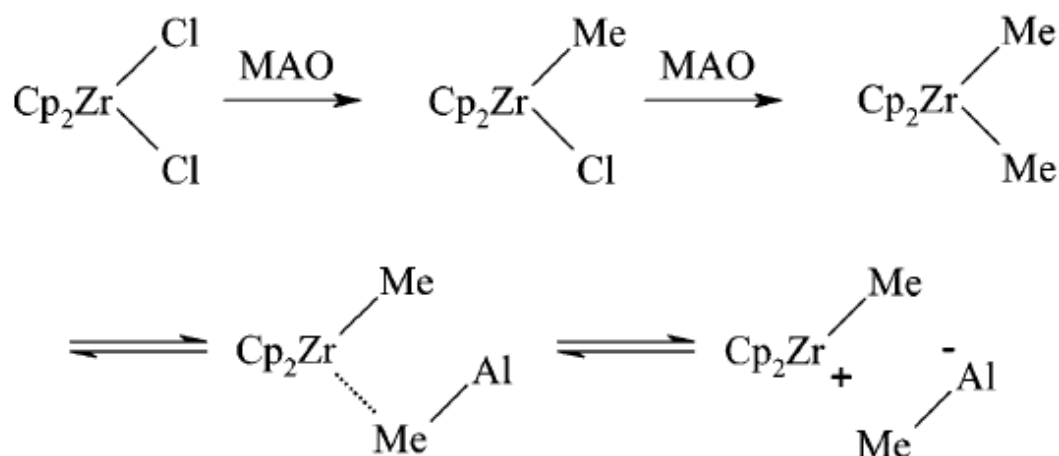
Scheme 1. Activation mechanism of metallocene [25]

1.3.2 Polymerization mechanism

Olefin polymerization takes place through insertion mechanism. The incoming monomer coordinated to vacant side of metal. For Insertion mechanism there should be present vacant active site on active metal centre for incoming monomer coordination and this process further continues through chain migration. Cossee proposed a two step insertion mechanism as in case 1 (Figure 3). Initially olefin approaches to the vacant site on active metal centre and finally migration of olefin chain take place. Green and Rooney also described two step polymerization mechanism based on oxidative addition of hydrogen to metal centre, forming the four centre metallacycle and in second step reductive elimination cause the final product. However Green and Rooney mechanism failed due to unsatisfactory explanation to the cations with d^0 and d^{14} electronic configuration because these systems have no available electrons for oxidative addition

of hydrogen. Mechanisms (3 and 4 in fig. 3) are modified versions of Green-Rooney mechanism which also present the agostic interaction within four centre transition state. [14]
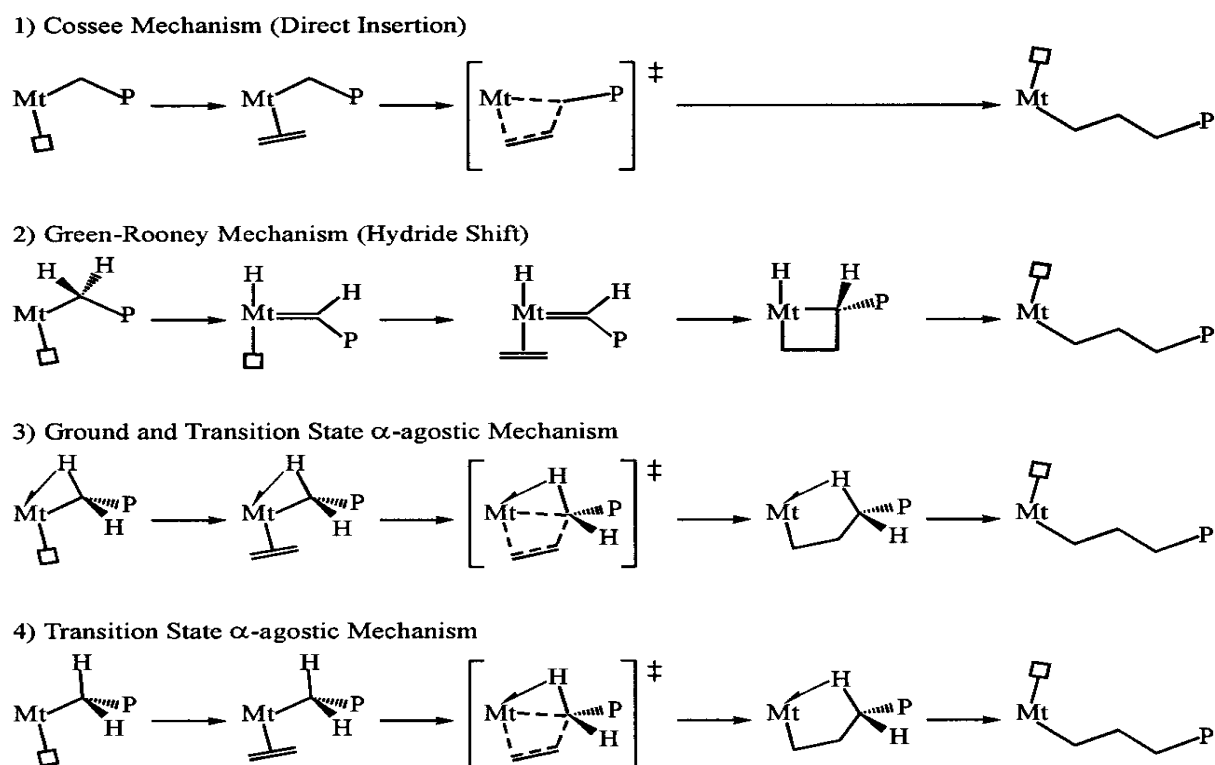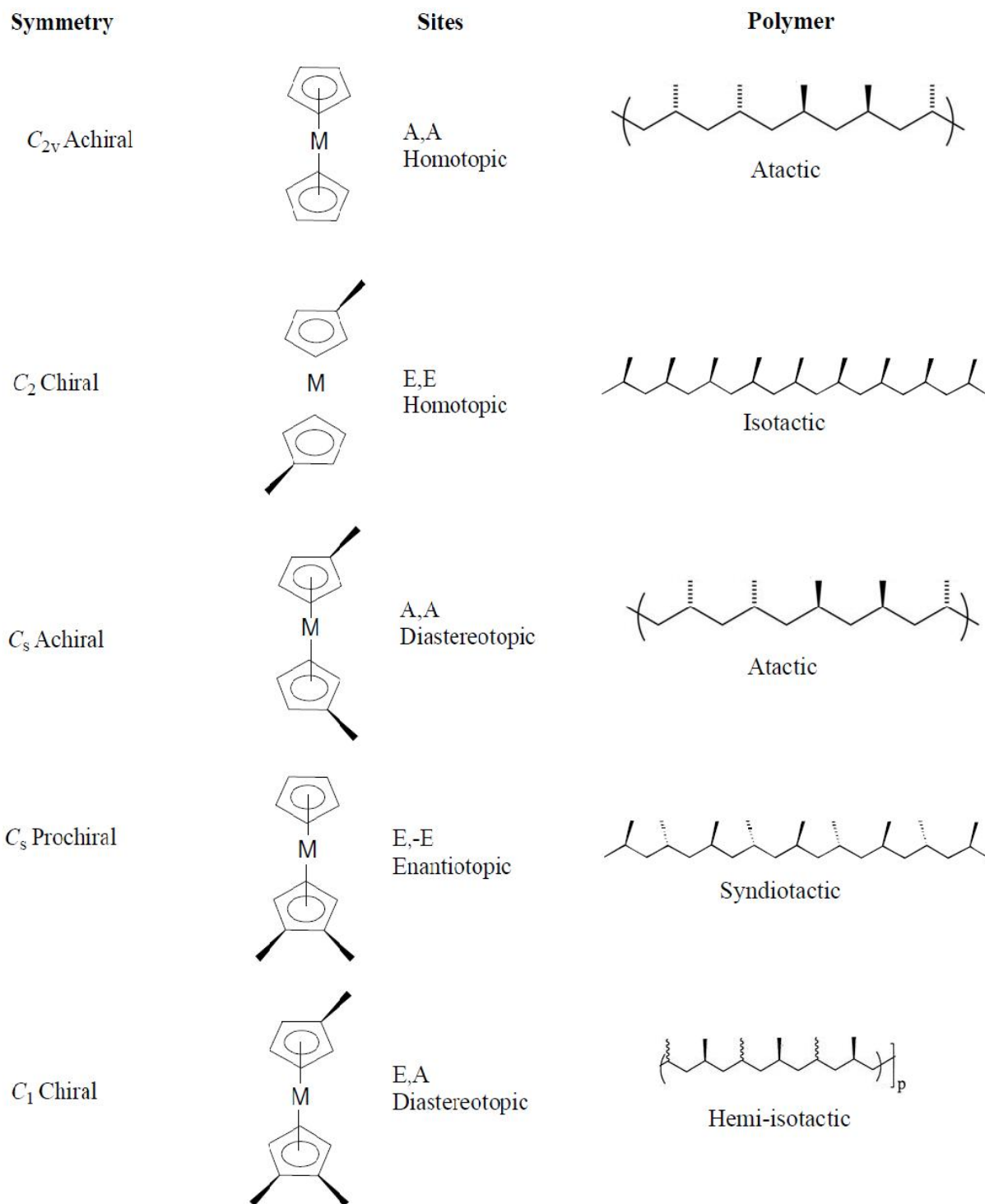
1) Cossee Mechanism (Direct Insertion)

2) Green-Rooney Mechanism (Hydride Shift)

3) Ground and Transition State α-agostic Mechanism

4) Transition State α-agostic Mechanism

Figure 3. Possible mechanisms of olefin polymerization [14]

1.4 Stereochemistry

Metallocene catalysts provide a good control of polymer microstructure and its related properties owing to catalyst structure. The configuration of the catalyst determines the stereoselectivity of monomer insertion which is directly link to stereochemistry of the polymer. Ewen *et al.*[19], [20] and Kaminsky *et al.*[21] reported series of stereo selective metallocenes structures to describe the stereochemistry of polymers. Figure 4 describe the influence of metallocene structure on polymer stereochemistry.

Metallocene active species contain two alternative active sites. Metallocene complexes possessing two nonselective sites produce mainly atactic polypropene. The last inserted monomer unit changes the nature of the corresponding site. Number of polymer microstructures directly related to the number of active sites. In Figure 4, C_{2v} achiral metallocene has two possible alternate positions for olefin insertion. It can produce atactic polymer (random insertion) while C_2 symmertic *ansa* metallocenes produce isotactic polymer by enantiomorphic control mechanism. *Cs* prochiral metallocene has two coordination sites with enantiotopic nature which forms syndiotactic polymer chain. C_1 chiral and C_s achiral metallocenes in Figure 4 have two

Symmetry	Sites	Polymer
C_{2v} Achiral	A,A Homotopic	Atactic
C_2 Chiral	E,E Homotopic	Isotactic
C_s Achiral	A,A Diastereotopic	Atactic
C_s Prochiral	E,-E Enantiotopic	Syndiotactic
C_1 Chiral	E,A Diastereotopic	Hemi-isotactic

Scheme 2. Ewen's Symmetry Rules (E = enantioselective site, A = nonselective site) [22], [23]

diasterotopic coordination sites; have ability to form hemiisotactic polymer chain rather than syndiotactic polymers. [22], [23]

1.5 Methylaluminoxane as Co-catalyst

MAO is amorphous white color powder or glassy form in toluene. It is highly pyrophoric and highly reactive for acidic proton carrying chemicals. The degree of oligomerization generally varies from 5-30 and molecular weight range is 250-1700. MAO exists in mixture form with TMA and offer difficulties in separating TMA from MAO.

MAO co-catalyst activity toward metallocenes was found to be higher than alternative aluminoxane cocatalytic systems such as ethylaluminoxane (EAO) and isobutylaluminoxane (IBAO). Large excess amount of MAO is applied for higher yield of polymers. However previous research give varying aluminum /transition metal ratios from 1000 to 50000 even with lower ratios. Experimental results revealed that that the rate of polymerization decreases as the TMA/MAO ration increases. Experimental evidence revealed its role as an alkylating agent and an impurity scavenger, formation of active sites and the prevention of their deactivation by bimolecular processes. [24]

Aluminoxane co-catalyst also imparts several drawbacks such as higher Al/Mt ratios are required to achieve good catalytic activities, relatively expensive reagent, structurally ill defined, variation in composition related to method of preparation, and a solution instability that increases with time. [15], [16] High cost and quantity required for polymerization compel the research to find some alternative co-catalyst rather than aluminoxane with a comparative activating ability. [17] Higher alkylalumoxanes (HAO) and tetraalkylalumoxanes (TAAO) have been reported in some cases as much more effective co-catalysts compared to MAO. However both commercial HAO and TAAO are not cheaper than MAO. [18]

It is desirable to explore some isobutyl analogues with less bulky substituents which are synthesized from relatively cheaper tri-isobutylaluminum. One of the most promising model of isobutyl related class is isobutylaluminoxane cage structure which contains both bridging hydride and three-coordinate aluminum sites. Hydrolysis of tri-*tert*-butylaluminum produces cage-type structures with four-coordinate aluminum sites. Cages consisting of six, seven, eight, and nine aluminums have also been structurally characterized by Wu *et al.* [19] Isobutylaluminoxane containing ring and ladder motifs are also successfully synthesized form (2,4,6-tri-*tert*butylbenzene-AlH$_2$)$_2$.

2 Specific Literature Part

2.1 Structures of MAO

Methylaluminoxane (MAO) is considered as the best co-catalyst for α olefin polymerization. However, knowledge of real MAO structure, its reaction sites and its participation to the activation process is still unveiled. Many theoretical and experimental efforts are being done to expose the structure of MAO. The general formula of MAO complex is $[-Al(CH_3)O-]_n$ with $n =$ 6–20. [25] The preliminary studies suggest the linear and cyclic structures with highly Lewis acidic tri-coordinated Al sites (Figure 1). Further studies favor the tetra-coordinated aluminum atoms present in cage and nano tubular structures based on crystal structure of $[Al_7O_6Me_{16}]^-$ anion demonstrated by Atwood *et al.* [26], [27], [28]
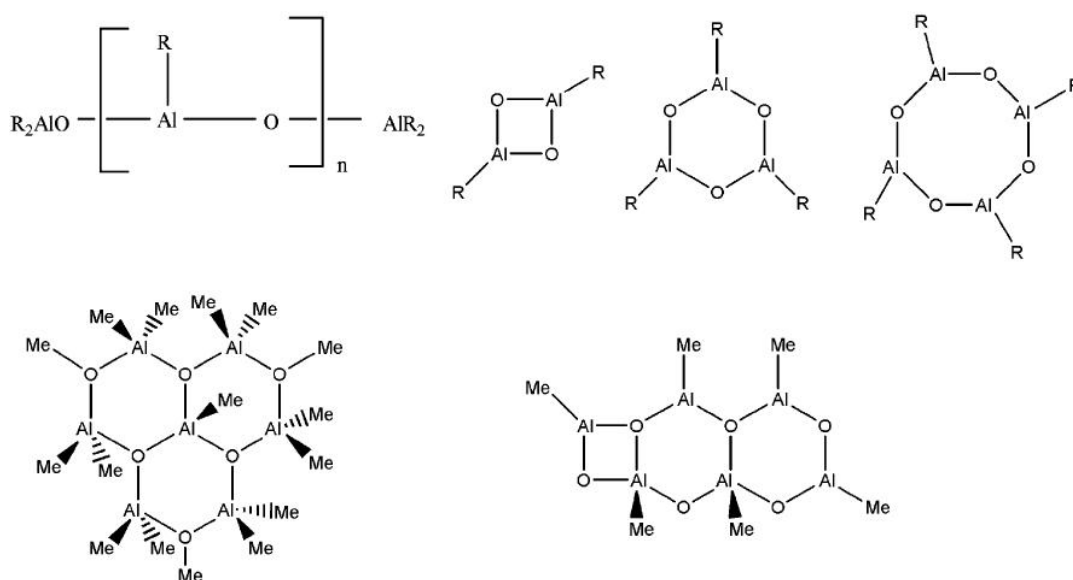

Figure 1. Linear and cyclic structures of MAO with tri-coordinated Al atoms [28]

Barron *et al.* [29], [30] characterized the MAO structures by substituting the methyl groups with bulkier *tert*-butyl groups. The synthesized structures confirm the three dimensional nature of MAO cage structures which are formed by tetra coordinated aluminum atoms bridged with tri-coordinated oxygen atoms. Sinn [32] described the formation of cluster cage structures by aggregation of $Al_4O_3Me_6$ trimers which were first proposed by Barron. [33] However potential models of MAO described by Hall [34], Ziegler [35] and Linnolahti [36], [37] are independent from $Al_4O_3Me_6$ trimer. Ladder type structures are formed by aggregation of DMAH $(Me_2AlOH)_n$ $(n=2, 3, ...)$ by trans-annular CH_4 elimination while cage structures $(MeAlO)_n$ are produced by reaction between the termini of ladder-type species. On the other hand, nanotubular structures are formed by coupling of cyclic oligomers $(Me_2AlOH)_n$ with CH_4 elimination. Intramolecular

elimination of CH_4 supports the growth of aggregates in Hall and Linnolahti MAO models. Figure 2 represents the MAO compounds studied by different researchers.
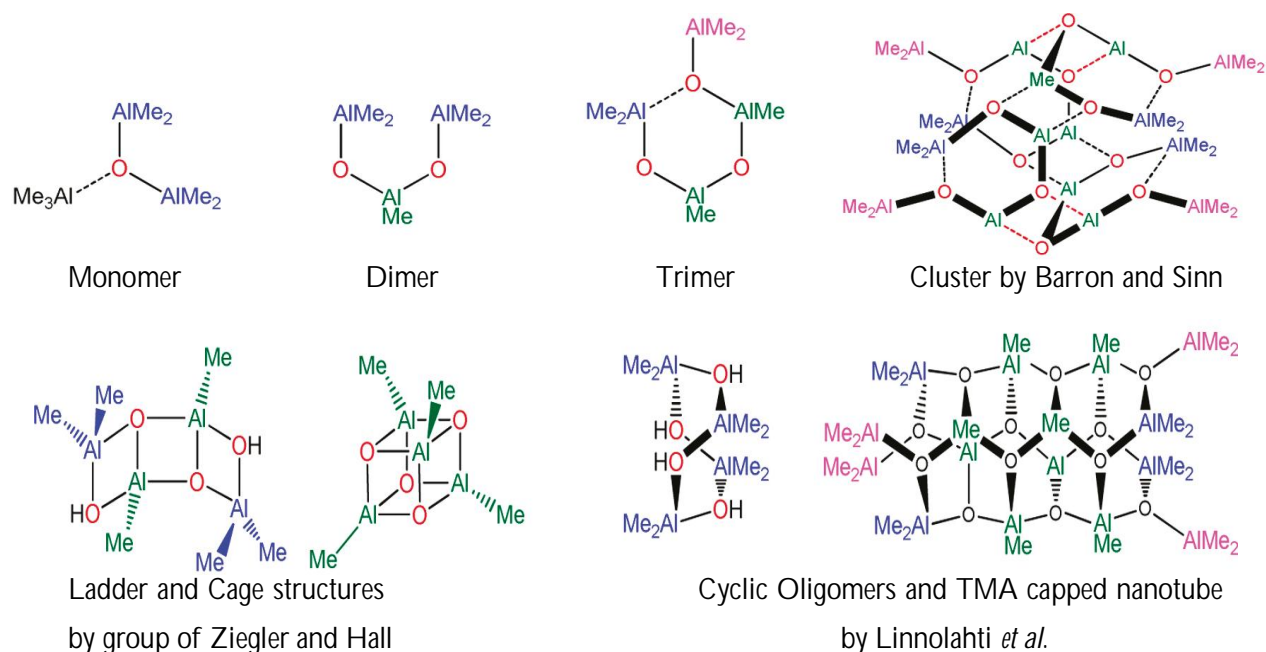

Figure 2. Purposed MAO models studied by Barron, Pasynkiewicz, Sinn, Ziegler, Hall, and Linnolathi [38]

2.2 Quantum Chemical studies on MAO

2.2.1 MAO models with three coordinated Al atoms

Systematic quantum chemical study was performed on three coordinated linear and cyclic MAO elementary fragments up to n=4 where n is degree of oligomerisation. Luhtanen *et al.* [25] differentiated the MAOs on the base of their short Al-O distances due to π bond interaction between aluminum and oxygen. In addition to π bonding, short bond length of Al-O is also associated to strong cationic character of tri-coordinated aluminum centre. It is also observed that π bonding is directly influenced by the presence of electron withdrawing substituents on aluminum atom. Al-O-Al linear bonds in open chain MAO structures is due to π bonding which is observed in the following structures (Fig. 3). In cyclic three-coordinated aluminum MAOs, Al-O bond distances are reduced with increase of number of elementary fragments (n). Relative stabilities of MAO structures were estimated in reference to TMA. Relative stability of open chain structures was found independent of n values while relative stability of cyclic structures is enhanced with size of ring. Higher relative stability of larger rings is associated to the less ring strains and it favors the formation of π interactions.
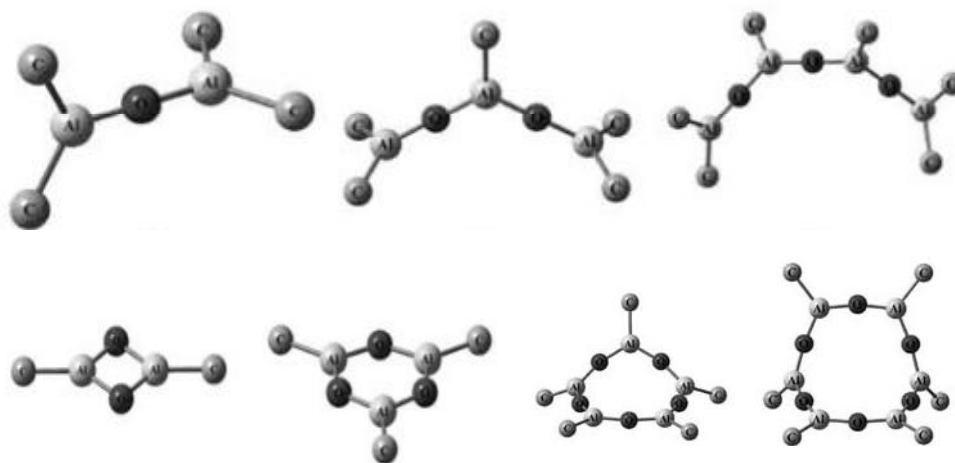
Figure. 3 Optimized Structures of Linear and Cyclic MAO elementary Fragments (n=4). Hydrogen atoms are omitted for clarity. [25]

Yamasaki [39] carried out *ab initio* calculations to study the Lewis acidity of different two and three coordinated Al-sites of MAO. Lewis acidity was determined in term of binding energies of chloride anions to the Al- site. Chloride ligand bonded to Al site either by σ bond or by bridged π bonds. It was reported that the oxo-bridged tri-coordinated Al- sites which have ability to form bridged structure with chloride ligand are generally more favorable than σ- coordinated chloride ligand. Acidic character of hexagonal ring Al- site is slightly increased with addition of further Al atoms. Further results suggest MAO-Cl⁻ anion should contribute approximately 100 kJ/mol energy to cationic centre for thermal stability of complex.

2.2.2 MAO models with four coordinated Al atoms

Experimental and theoretical studies reveal that Al atoms with four bonds are more stable than trigonal structures. Dative bonds between O $\rightarrow$Al atoms give rise to the formation of three dimensional cage structures of MAO. Ystenes *et al.* [40] have evaluated the three dimensional cage structures of MAO $(AlCH_3O)_9$ based on IR spectroscopic and DFT calculations. This MAO model comprised of four and six member rings.
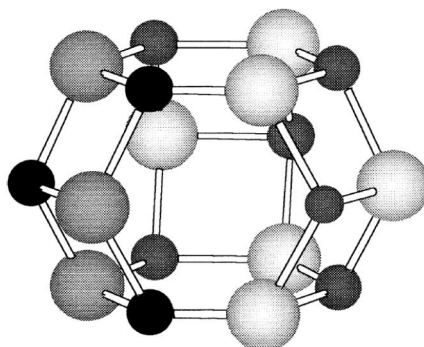

Figure 4. cage structure of MAO with $(AlCH_3O)_9$ formula; purposed by Belellie et al. [42]

Hexagonal rings formed the upper and bottom part of the cage structure with a regular C_{3h} symmetry. [41] Ivan and Valdimir [43] have applied DFT approach to identify the real MAO cage structures with oligomerization degree n= 4-15. They found that MAO cage structures with n $\geq$ 6 are thermodynamically and electronically promising models. The composition of these cage MAO were found to be good agreement with the NMR spectroscopic data in which Al atoms are bonded to oxygen atoms. The calculated triple layer cage structure with n=12 has penta and tetra-coordinated Al atoms which are present in inner and outer layer of the cage structure respectively as shown in Figure 5. These MAO were consistent with the Barron´s triple layer cage structures in which all the Al atoms are tetra-coordinated.
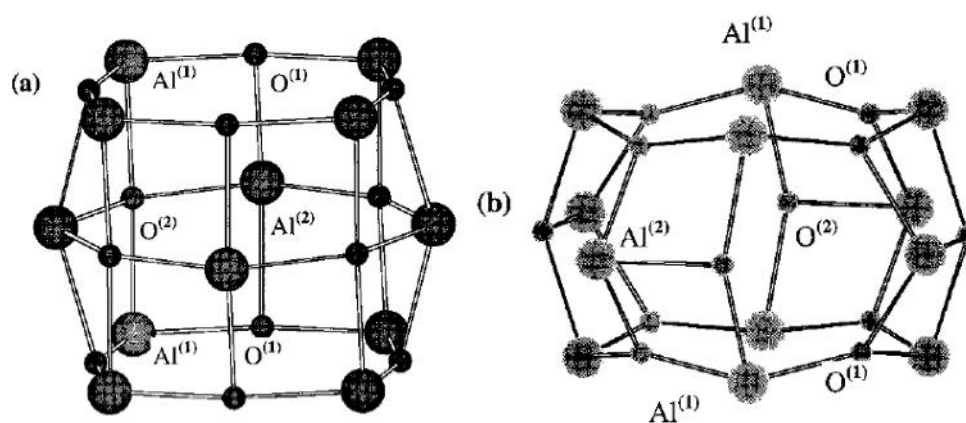

Figure 5. Triple layer Cage structure (AlMeO)$_{12}$. Al^2-O^2 bonds are equivalent in a while non-equivalent in (b). Methyl groups of MAO are omitted for clarity [43]

In above structure all the three coordinated oxygen atoms form the dative bonds with tetra-coordinated aluminium atoms. It means each oxygen atom is bonded to three (CH_3-Al) groups and vice versa. These classic models were identical to the experimentally verified tert-butyaluminoxane cage structures. [41] Later on Earley [27] has performed DFT calculations on cyclic and cage MAO models which are in agreement with the previous work. DFT calculations favor the formation of cage structures composed of tetra-coordinated aluminum atoms, whose IR spectrum was found to be in agreement with the previous experimental data.

2.2.3 Nano-tubular MAO Models

Nano-tubular MAO structures were also proposed which are thermodynamically more stable than reference cage structure $Al_{28}O_{28}H_{28}$. Hydrolysis of TMA gives a variety of MAO nanotubular structures which named after the arrangement of carbon nanotubes (Fig. 6). Armchair (2,2) dodecamer ($Al1_6O_{12}Me_{24}$) appears to be a possible structural feature of real MAO with two active sites present at tube ends. The bridging pentavalent carbon bond (Al-C) breaks to form the active tri-coordinated Al site which has shown the ability to abstract the methyl ligand from metallocene. Recent theoretical investigation suggests that nano-tubular MAOs might be the active species for olefin polymerization. [36], [37]
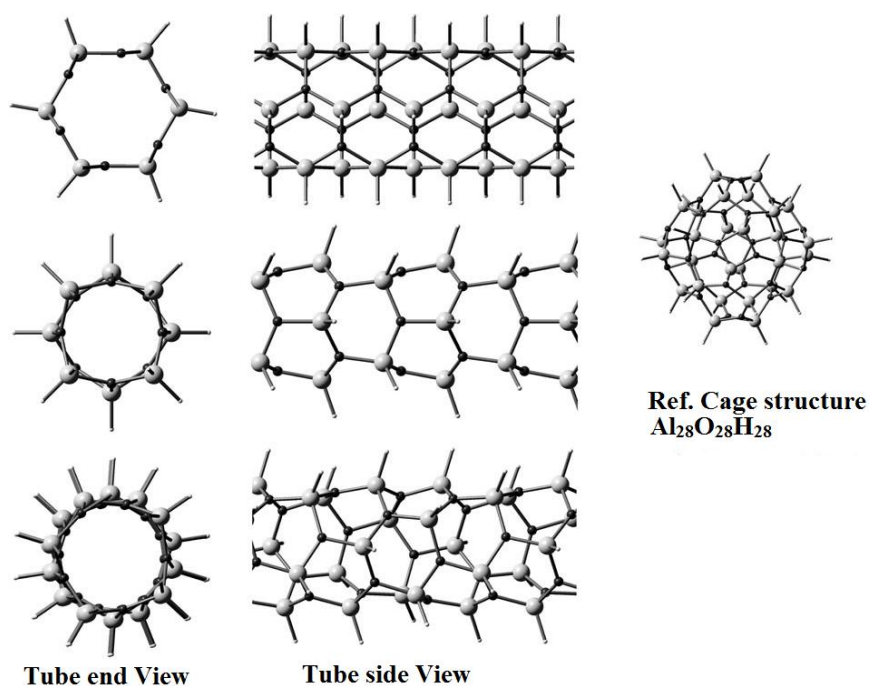
Figure 6. Optimized structures of the favored [AlO(H)]ₙ nanotubes of infinite length for each family: armchair (3,3) (top), zigzag (4,0) (middle), and chiral (4,1) (bottom) [37]

2.3 True and Classic MAO Structures

MAO structures are classified into two groups on the basis of chemical composition which is often referred to Al:CH$_3$:O ratio. "True" MAO structures have Al:CH$_3$:O = 1: 1.5 : 0.75 ratio while "Classic" models have Al :CH$_3$:O = 1:1: 1 ratios. There is contradiction present among experimental and theoretical results regarding actual composition of MAO. 1.4 to 1.5 ratios are most abundant among scientific literature however values beyond the above limits are also found. [10], [44] Ivan and Valdimir [43] described the reversible process of formation of true and classic MAO structures.TMA molecule reacts with the most reactive Al^2-O^2 site in classic MAO through concerted mechanism. During chemical reaction, TMA cleaves the Al^2-O^2 bond in MAO molecule by transferring the methyl group of TMA to Al^2 while Al(CH$_3$)$_2$ forms bond with O^2 atom. The calculated structures of true MAO are consisted with the previous described MAO structures by Sinn *et al.* [32] Figure 7 represents the exothermic reaction between TMA (2, 3, 4) and MAO with n = 6, 9, 12 respectively.
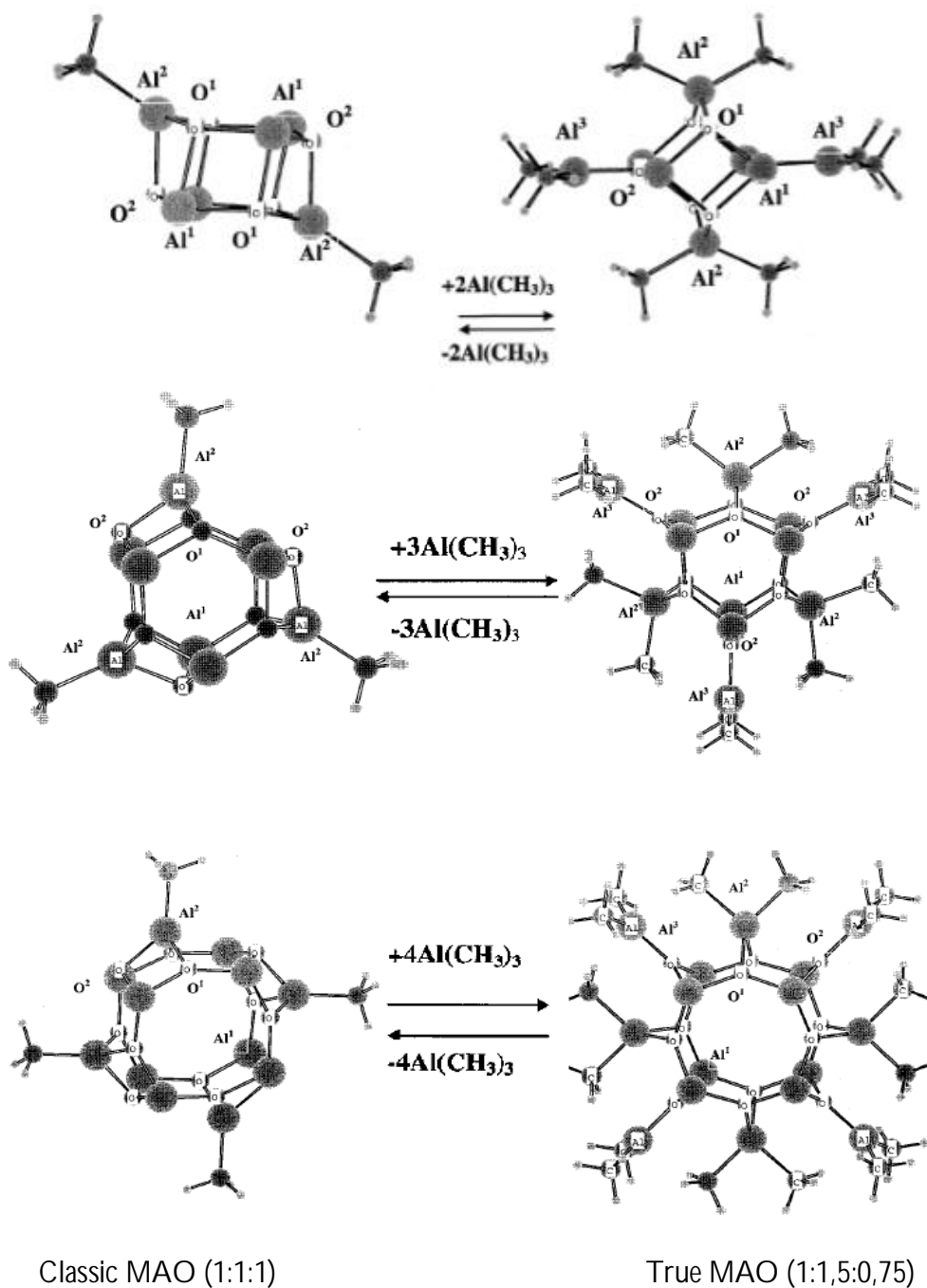
Figure 7. Reversible reaction of Classic and True MAO along with Al:CH₃:O ratio (methyl groups of MAO in outer layers are omitted for clarity) [43]

2.4 TMA-MAO Interaction

Commercial solution of MAO exists as combination of MAO oligomers and TMA. It has been considered that high TMA contents improve the co-catalytic activity of MAO by enhancing the life time of MAO however it depress the molecular weight of polymer to a large extant. [44] Previous literature studies show that there exist a dynamic equilibrium between TMA and MAO.

[45], [46] In this regard, Zurek *et al.* [47], [28] have investigated the dynamic equilibrium of $(AlOCH_3)_n$ oligomers which consists of TMA and MAO components. In this study, bonding nature of TMA to MAO and respective TMA/MAO ratios were evaluated. This was done by adding TMA molecules to MAO. It was found that TMA bonds to O atoms by breaking a strained acidic bond. $AlMe_2$ group bonded to O and one methyl group is transferred to corresponding Al atom. Theoretical results suggested the lower TMA contents present in MAO oligomers. The addition of more than one TMA molecules energetically destabilized the cage structures. Moreover TMA contents were increased at higher temperatures which indicate that smaller structures are entropically more stable. The resultant pure MAO structures were in agreement with the Barron´s structures. [30] The stability of these structures was described in term of binding nature of MAO constituent atoms. Four types of binding environments were reported with in cage structures based on hexagonal (H) and square rings (S). Stability of these MAO structures depends on type and boding nature of atoms and stability order was found as 3H > 2H + S > 2S + H > 3S.

Eilertsen *et al.* [48] investigated the interaction between TMA and MAO. It was thought that there exist a dynamic equilibrium between TMA and MAO molecules and further addition of TMA cause to dissociate the MAO structures into small fragments. FTIR spectroscopic studies were carried out to investigate the effect of temperature and further addition of free TMA to MAO solutions. IR spectra of free and MAO with 5% TMA addition up to 50% were illustrated in Figure 8. On the base of experimental results it was concluded that there is no interaction or dynamic equilibrium present between TMA and MAO molecules. The co-catalytic activity of TMA depleted -MAO was tested with Cp_2ZrCl_2 pre-catalyst which gave the similar results to the commercial MAO solution.

TMA-MAO interaction was also analyzed by mass spectrometry in which MAO samples were heated at 50∘C to 450∘C and gaseous product was formed. Characterization of gaseous product was done by mass-spectrometric (MS) method which reveals the formation of methane gas. During cooling process, condensed material was obtained formed on the cell wall which was analyzed by proton NMR method which indicates the release of TMA from MAO on heating. High temperature causes to dissociate MAO through protolysis reaction and facilitates the transformation of true MAO to real MAO which is supported by the change in CH_3/Al ratio from 1.6 to 0.9. [41]

2.5 MAO supported on Silica

MAO characterization can be amplified in solid form. This idea led to the development of supported homogenous metallocene catalyst which is an active area of research nowadays. Homogenous metallocene catalyst solution is suitable for high pressure manufacturing plants but this does not work well for gas or slurry phase processes. Hybrid sol-gel, silica or alumina supported homogeneous metallocene catalysts are employed in gas and slurry phase polymerization reactors for better yield. However immobilization of catalytic components on supported surfaces lowers the catalyst activity. Incomplete activation of the catalyst, limited

monomer diffusion to growing polymer chain is responsible for lower yield of polyolefin. The percentage yield can be enhanced by pre-contacting MAO-zirconocene which forms the activated species before immobilization on silica and this system shows higher catalytic activity. [45], [46], [49]
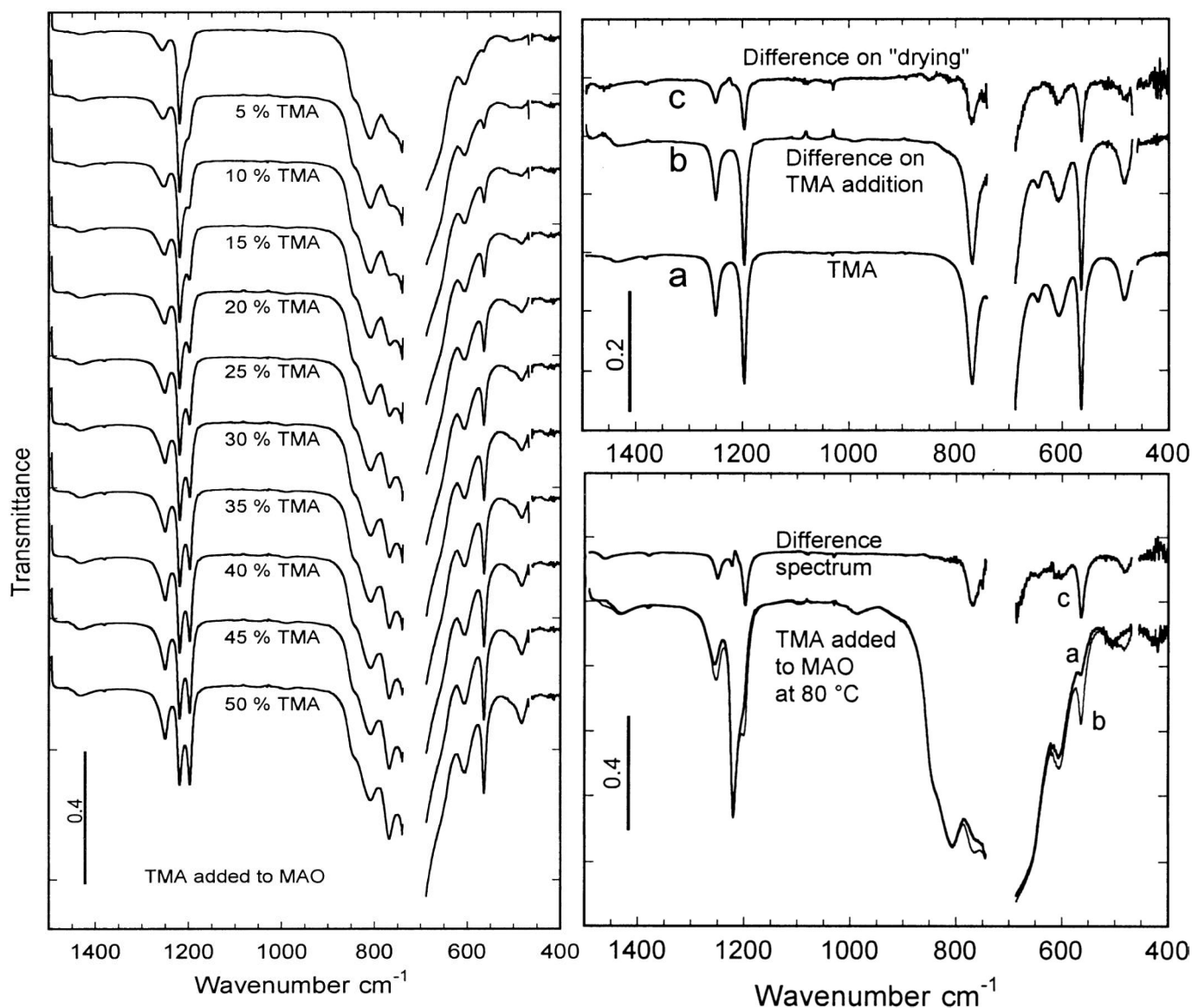

Figure 8. IR spectrum of TMA-depleted MAO-top and the same solution after repeated additions of TMA (Left). TMA components in TMA–MAO mixtures. a. TMA only. b. changes in spectra when TMA is added to TMA-depleted MAO. c. Component removed by drying (Right). The toluene spectrum has been subtracted. The region around 700cm-1 has been removed because of noise. [48]

Eilertsen *et al.* [48] utilized different instrumental techniques to characterize the immobilized MAO structure, its bonding with silica and co-catalytic activity. MAO toluene solution with 0.5–20.0

wt.% Al/SiO$_2$ ratio was employed to modify the silica surface. Inductively-coupled plasma-optical emission spectroscopy (ICP-OES) indicates that Al atoms are not directly bonded to silica surface.

X-ray photoelectron spectroscopy (XPS) was applied to evaluate the surface constituent atoms of catalyst e.g. Si, O, C and Al and their characteristic binding to surface. Atomic concentration over modified silica surface was determined in term of Al/Zr ratio which decreases as a function of surface depth. XPS spectrum of MAO-supported silica is illustrated in Figure 9. Al contents over silica surface are increased as the MAO concentration is raised in impregnation solutions.
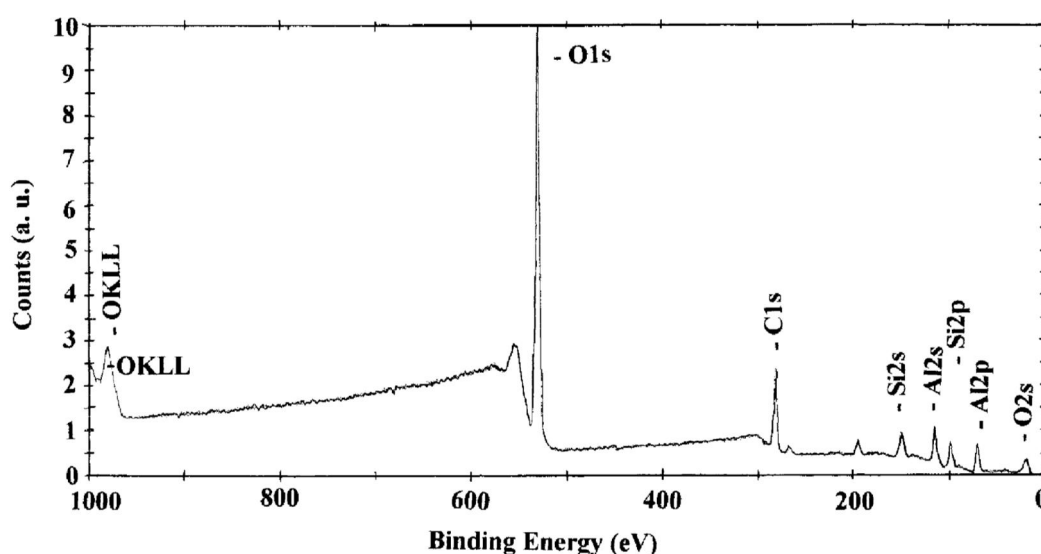
Figure 9. XPS spectrum of MAO/SiO$_2$ (4.0 wt.% Al/SiO$_2$)[46]

Silicon and aluminum 2p core level spectra of silica supported MAO was illustrated in Figure 10. Two peaks were observed in silicon 2p core spectrum (left) at binding energy (BE) of 103.3 eV and 101.1 eV. Major absorption peak (103.3 eV) indicates the bulk silica atoms while lower broad peak (101.1 eV) is associated to surface Si atoms. Lowering of BE of Si atoms is proportional to the reduction of electron density of silica surface atoms due to increase of Al contents. The noise peaks in both spectra correspond to heterogeneity of the surface composition due to MAO concentration. First two Al 2p core level spectra (a,b) represents the unsaturated surfaces with MAO while broad peak (c) is observed with MAO saturated surface. Low BE curve represents exposed Al species at outer surface regarded as active atomic sites in polymerization.
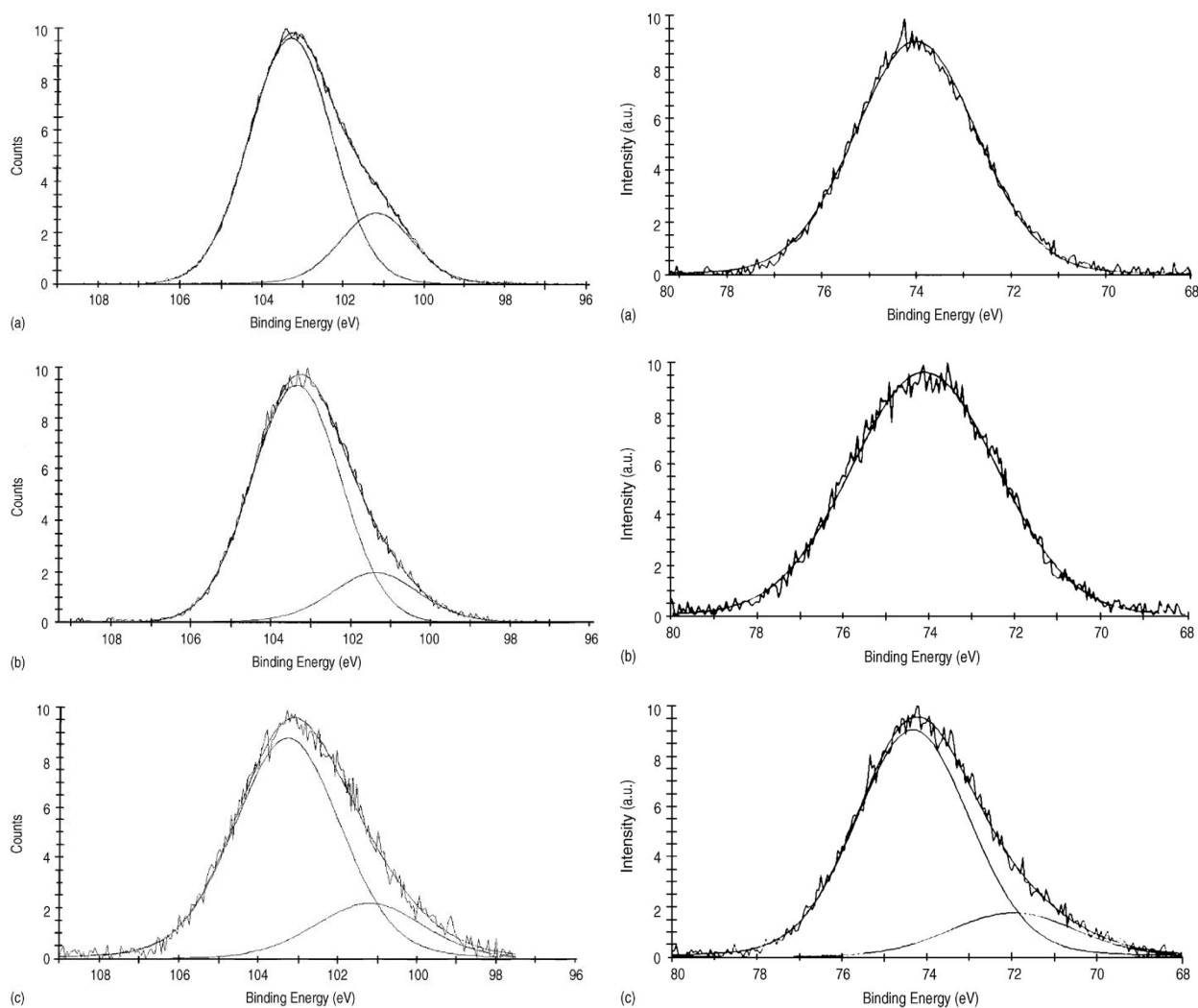
Figure 10. 2p core level spectra of Si (left) (a) SiO2; (b) 0.5 wt.% Al/SiO2; (c) 20.0 wt.% Al/SiO2. and Al (right) (a) 0.5 wt.% Al/SiO2; (b) 4.0 wt.% Al/SiO2; (c) 10.0 wt.% Al/SiO2.for MAO/SiO2 supported system. The line with a visible noise component is the experimental raw data [46]

Silica supported MAO surfaces are analyzed by UV–VIS spectrometer within 200–560 nm UV range (Figure 11). Sharp absorption band is observed at 271 nm with a shoulder at 289 nm for 0.5 wt.% Al/SiO$_2$. Higher concentration of MAO produces two intense bands at 269 and 286 nm which are associated to rise in Al contents. These results match with the absorption spectrum of MAO in benzene solution at 286 nm taken at room temperature. [50] The bathochromic shift is associated to the interaction of Al and non-bonding electrons of bridged oxygen atoms. This phenomenon of decrease in electron density is also in agreement with the low BE signal in XPS spectra for higher Al contents.
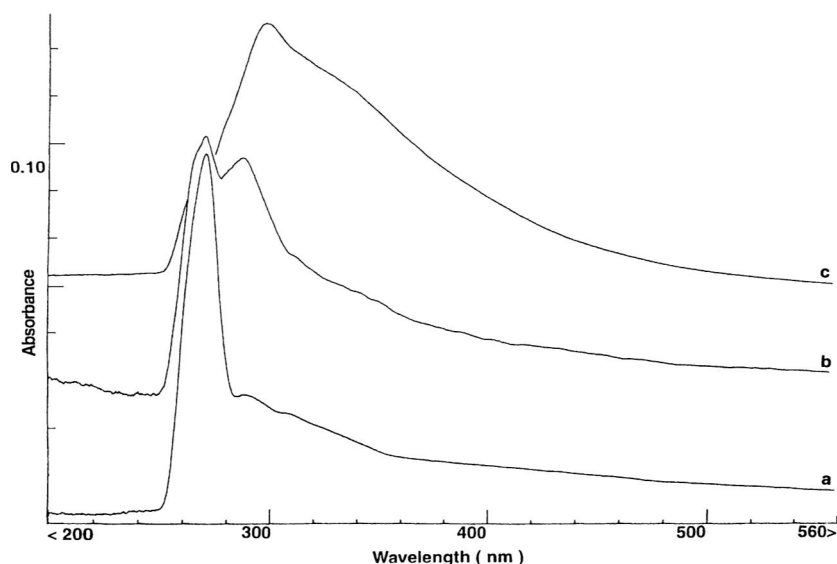
Figure 11. UV–VIS spectra of MAO-modified silica at room temperature: (a) 0.5 wt.% Al/SiO$_2$; (b) 10.0 wt.% Al/SiO$_2$; (c) 20.0 wt.% Al/SiO$_2$. [46]

Absorption band	Wavenumber (cm^{-1})
H$_4$OSi (Silanol)	3746
CH$_3$ (MAO) υ_a	3050-2810
CH$_3$ (MAO) υ_s	2950-2750
Al-CH$_3$	2940, 2900, 2830
Si-CH$_3$	2960, 2900
MAO content	2840
Intraglobular OH	3650-3200
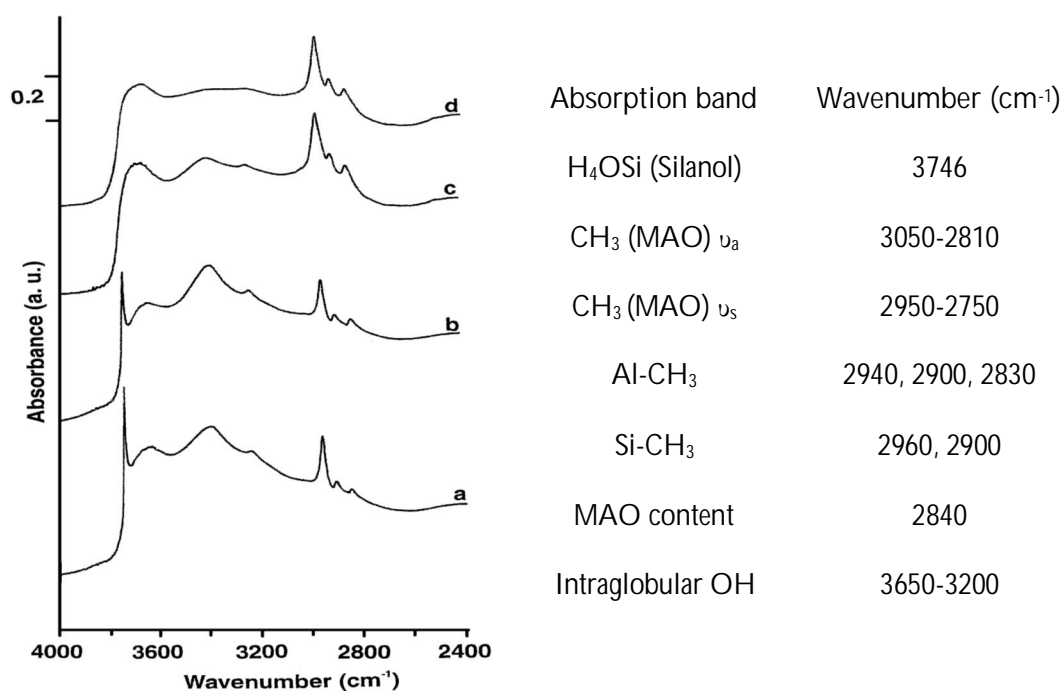
Figure 12. DRIFTS spectra of MAO-modified silica measured at 40 °C: (a) 0.5 wt.% Al/SiO$_2$; (b) 2.0 wt.% Al/SiO$_2$; (c) 10.0 wt.% Al/SiO$_2$; (d) 15.0 wt.% Al/SiO$_2$. [46]

MAO absorbed silica surfaces are analyzed by diffuse reflectance infrared spectroscopy (DRIFTS) and corresponding spectrum and absorption bands are shown in Figure 12. Silanol molecules give a sharp band (3746 cm^{-1}) in presence of low amount of MAO and disappear at higher concentration. This suggests the interaction of TMA and OH, producing complex species which enhance the heterogeneity of surface. The complex species compose of Al-CH$_3$ and Si-

CH$_3$ groups which give three and two absorptions bands respectively in C-H region of IR spectrum. Silanol also reacts with MAO which produces Si-CH$_3$ at 2960 cm^{-1}. Terminal methyl groups of MAO are sensitive to intermolecular interactions and their absorptions peaks are observed in 3000-2800 cm-1 range. Increase in MAO contents broad the absorption spectrum which is associated to the heterogeneity of surface composition. Absorption bands at 3395 and 3240 cm-1 are resulting from intraglobular OH groups and absorption band intensity is decreased due to intramolecular interaction of OH with oxygen of MAO molecules. Consumption of silanol OH group leads to higher catalytic activity of supported system.
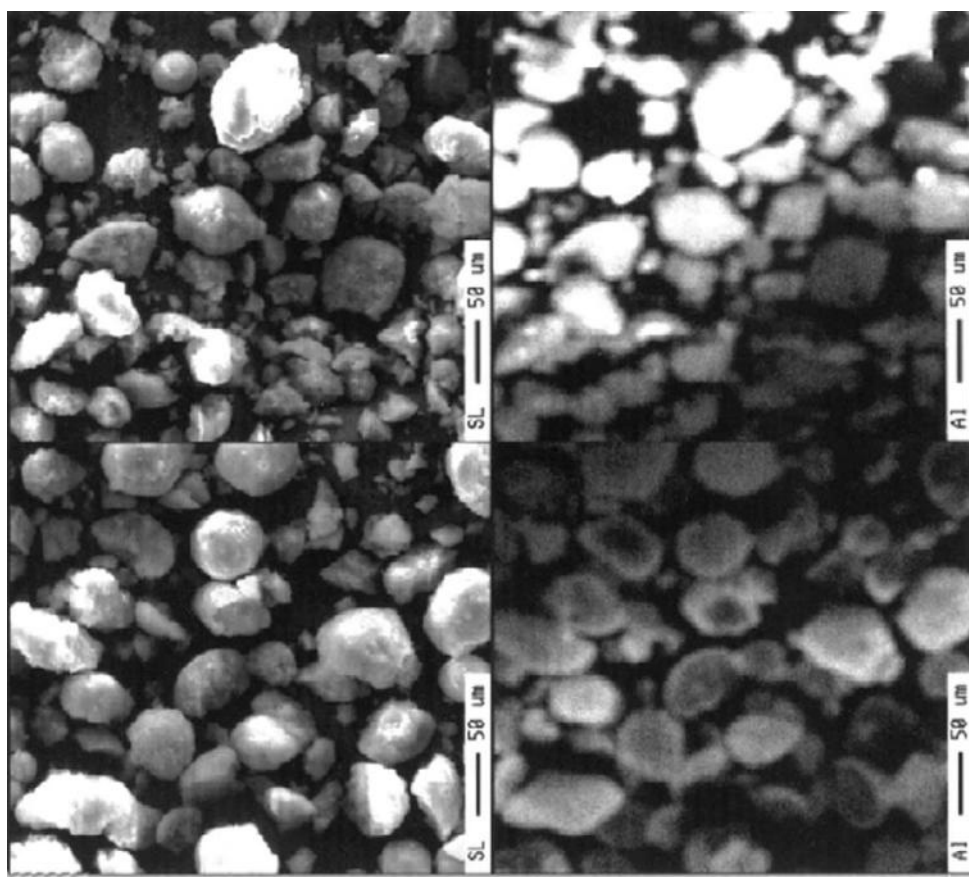
Figure 13. SEM photographs of MAO-modified silica (left) and element distribution map of Al by EPMA in the resulting solids (right): 4.0 wt.% Al/SiO$_2$ (bottom); 15.0 wt.% Al/SiO$_2$ (top). [46]

SEM diagrams (Fig. 13) of saturated and unsaturated MAO-modified silica show irregular distribution of fine particles over silica surface. Spatial distribution of metal atoms was evaluated by electron probe microanalysis EPMA. Bright area of EPMA photograph indicates the finely divided aluminum atoms.

Pol *et al.* [45] have investigated the interaction of supported metallocene and MAO by using FT-Raman spectroscopy. Vibrational spectroscopic information of breakage of Zr_/Cl and Zr_/Me bonds in metallocene can give the insight of formation of cationic centre by MAO. The experimental spectrum was calibrated with the help of *ab initio* calculations of vibrational

spectrum. The neutral dimethyl complex and cationic centre gave the spectral lines in 420-470 cm^{-1} region

2.6 Function of MAO

The key roles of MAO as cocatalyst are; (1) alkylation of a metallocene precursor like Cp_2ZrCl_2, (2) generation of a cationic zirconocene complex by abstracting chloride (3) stabilization of cationic complexes acting as counterion (4) re-activation of deactivated sites (5) water and oxygen milieu scavenger. The co-catalyst activation reactions with metallocene to form activated catalytic centre are given as

$$Cp_2ZrCl_2 + MAO-CH_3 \rightarrow Cp_2ZrClCH_3 + MAO-Cl \qquad (1)$$
$$Cp_2ZrClCH_3 + MAO \rightarrow Cp_2ZrCH_3^+ + \cdots MAOCl^- (active\ site) \qquad (2)$$
$$Cp_2ZrCl_2 + 2MAO-CH_3 \rightarrow Cp_2ZrCH_3^+ + \cdots MAOCH_3Cl^- (active\ site) + MAO-Cl \qquad (3)$$
$$Cp_2ZrCH_3^+ + MAOCl^- \rightarrow Cp_2ZrCH_3^+ \cdots MAOCH_3Cl^- (active\ site) \qquad (4)$$
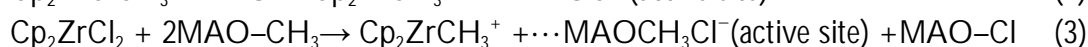
Equation (1) involves the alkylation reaction of dichloride zirconocene, which forms methyl chloride zirconocene precursor and MAO-chloride complex. The second step involves the formation of active centre by the breakage of chloride ligand from metal atom. The chloride anion is shifted to MAO due to the Lewis acidic character of MAO. $Cp_2ZrCH_3^+$ and MAO–CH_3Cl^- ions are produced by this reaction. Equation three represents the overall reaction while equation four describes the stability of ionic reactants rather than isolated ionic components. Theoretical investigations predict that MAO–CH_3Cl^- co-catalyst anion produce steric constrain and charge distribution in the metallocene cation.[28], [41], [46]

2.7 Characterization of MAO

Several experimental techniques are employed to solve the MAO structure. Although NMR spectroscopy is considered as a sophisticated technique for chemical characterization however disproportionation reactions and dynamic equilibrium of MAO solution are the failures of NMR analysis. However NMR along with other spectroscopic methods has been applied to investigate the size range of MAO oligomers and reaction mechanism. Moreover, X-rays diffraction does not work well due to difficulties in preparing isolated crystal samples. [28] [47] Higher reactivity of MAOs was due to presence of 2-3 acidic sites which are incorporated in oligomerization. The existence of dynamic equilibrium among MAO oligomers do not allow crystallization for x-rays analysis. [46] First crystallographic evidence about tetra-coordinated aluminum atoms was demonstrated by Atwood *et al.* [26] in 1983. Later on three dimensional MAO cages were further evaluated by Mason *et al.* [29] in relation to open cage structures of iminolanes.

2.7.1 NMR Spectroscopy

Ueyama *et al.* [51] characterized the dialkylaluminum oxides which were prepared by hydrolysis of TMA. It was found that methyl protons of [-O-Al(CH$_3$)-]$_n$ give a broad band at -3.35 ppm. The broadening of MAO spectrum is associated to coexistence of linear and cyclic structures. Imhoff *et al.* [52] have reported a rapid and accurate approach to characterize and estimate the product quality by measuring the residual amount of TMA in given solution of MAO. TMA and MAO peaks were resolved by adding excess amount of THF-d_8. Proton NMR spectra of MAO in toluene is shown in Figure 14. Residual amount of TMA can provide structural insight of MAO and number of methyl groups per aluminum atoms which is related to the molecular formula of MAO. This approach also limits the number of possible structures.
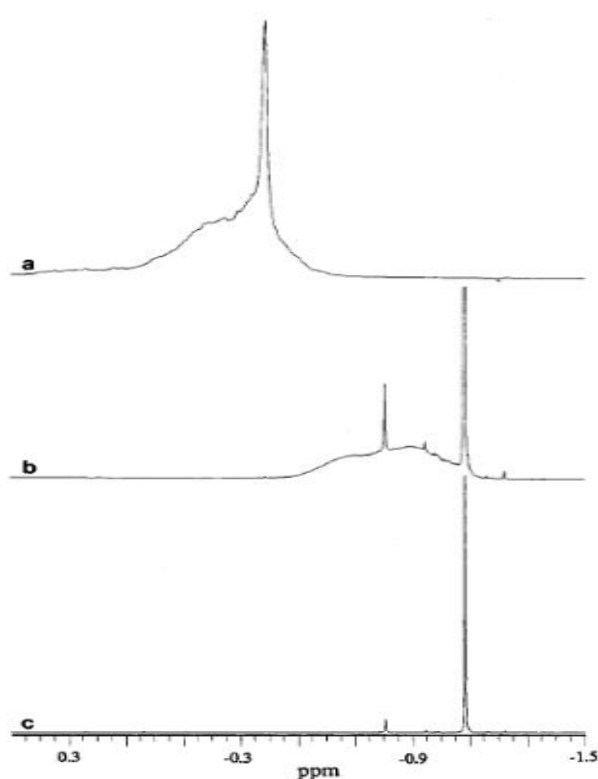
Figure 14. Proton NMR spectra of 30% MAO in toluene (400 MHz; 0.5 to -1.5 ppm). (a) Sample diluted in perdeuteriobenzene only. (b)Sample diluted in THF-d8. (c) Base line correction of b by curve fitting [52]

Fig. 14a represents the broad and featureless MAO peak. The TMA peak (-0.37 ppm) is superimposed on MAO peak (0.5 to -0.7 ppm). Approximately four volume of THF-d_8 has been added to same sample which cause slight upfield shift to MAO peak and TMA-MAO peaks are resolved at -1.08 and -0.3 to 1.3 ppm respectively (b) and Figure c shows the baseline correction of MAO on both side of TMA. The small peak at -0.8 ppm corresponds to low-molecular weight species or end group from the MAO. ^{1}H-NMR is a powerful tool to investigate the MAO quality during manufacturing process to final product.

Giannetti *et al.* [53] have reported the sharp resonance peak for TMA at -7.28 ppm while intense and broad peak for MAO at -6.55 ppm. Broadening and down-field shift of methyl carbon is in accordance with quadrupolar coupling with Al nucleus and inductive effect of oxygen atom respectively.
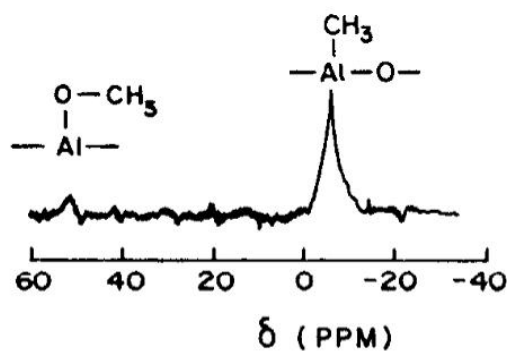
Figure 15. ^{13}C-NMR spectrum of MAO in benzene-d$_6$ [53]

Al atoms in MAO are considered as active site for co-catalytic activity and that´s why ^{27}Al NMR analysis has been performed by many researchers in different times. T. Sugano *et al.* [54] have investigated the several MAO models by ^{27}Al NMR spectroscopy. Methylalumoxane (MAO) and ethylalumoxane (EAO) broad peaks were observed at approximately 152 ppm with line widths at 1400 Hz and 2320 Hz respectively.
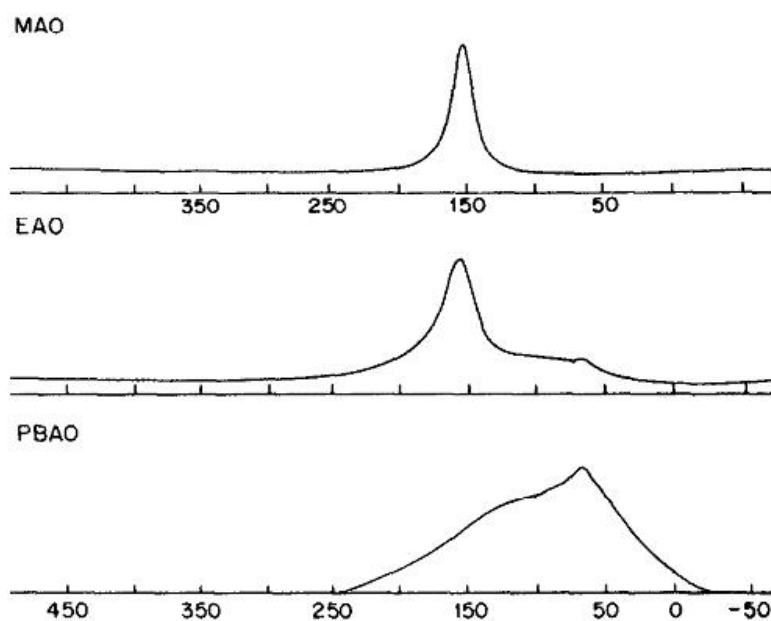
Figure 16. ^{27}Al-NMR spectrum of aluminoxanes [54]

^{27}Al NMR spectra revealed the tetra-coordinated nature of aluminium atoms which can freely move in toluene solution however chemical shift values of aluminium atoms in isobutylalumoxane (PBAO) are 66 ppm/570 Hz and 78 ppm/9960 Hz which is quite different from MAO case. This data suggests the different coordination structure of aluminium atom in isobutylalumoxane (PBAO) than MAO and EAO.

NMR spectroscopic evaluation suggested the dynamic structure of MAO and TMA. It was found quite difficult to separate TMA from MAO. The experimental results were also to be found in agreement the theoretical efforts.

2.7.2 IR Spectroscopy

Giannetti et al. [53] have also investigated MAO structures by IR spectroscopy. Their experimental data revealed that IR spectrum of [-O-Al(CH$_3$)-]$_n$ had intense absorption region around 800 cm^{-1} due to Al-O-Al stretching vibrations.

IR spectrum of MAO dried sample at 50 ^{0}C have been reported by Panchenko et al. [41] (Fig.17) which was obtained by diffusion reflection mode (DRIFT) spectroscopy. The low-frequency region A represents the characteristic stretching vibrations of Al-O bonds ranging from 870 to 950 cm-1. IR spectrum peaks at 1220 and 1250 cm−1 correspond to umbrellas vibrations of CH3-groups.
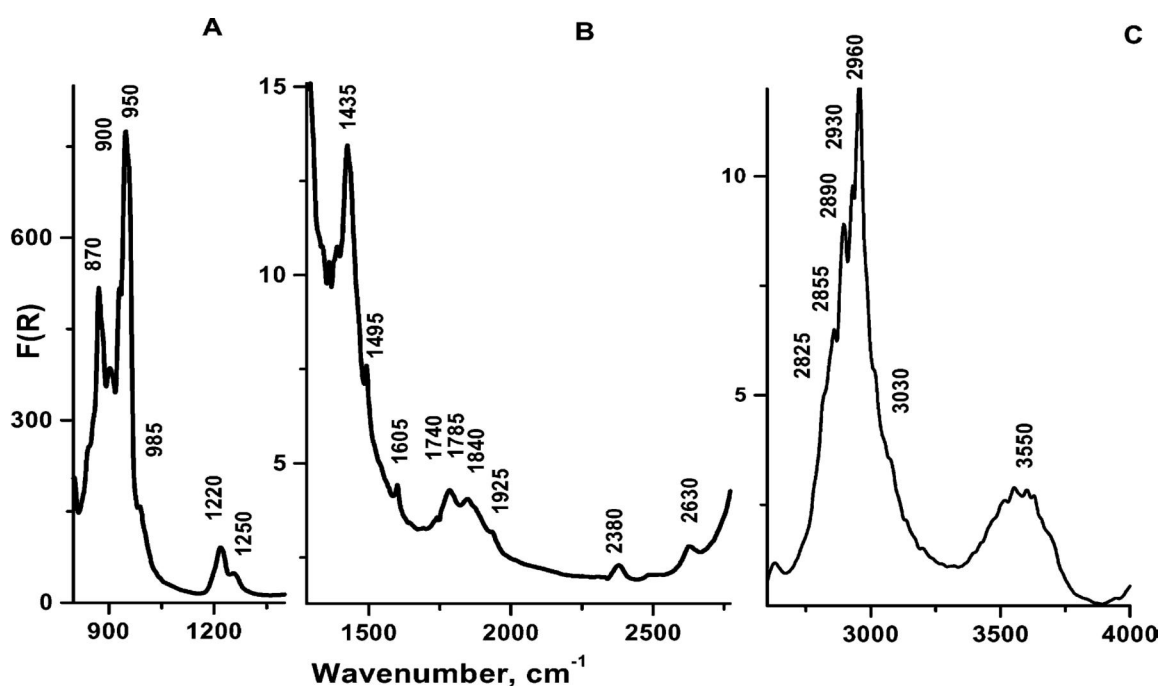
Figure 17. DRIFT-spectrum of solid MAO sample heated in vacuum at 50◦C [41]

Toluene also gives characteristics absorption bands of aromatic ring at 1495 and 1605 cm-1 (B). MAO sample dried over 50 ^{0}C temperature is unable to produce toluene characteristic peaks. C-H stretching vibrations of CH$_3$ groups are observed at 2700-3000 cm-1 absorption frequencies.

Four characteristic bands exhibit the presence of terminal and bridged methyl groups in MAO structure in which bridged methyl molecules are responsible for higher reactivity of MAO than terminal methyl molecules.
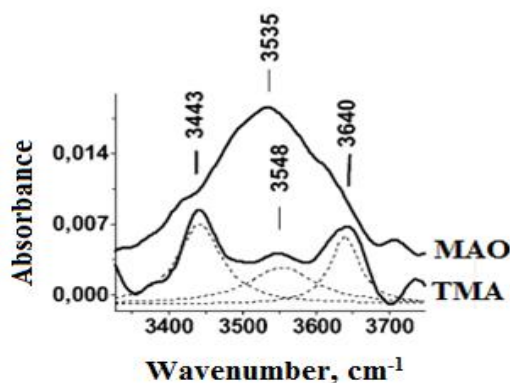
Figure 18. IR-spectrum of toluene solutions: (1) TMA (0.23 M); (2) MAO (1.42 M)[41]

IR spectrum of TMA and MAO in toluene solution was also reported (Figure. 18). Broad absorption band at 3535 cm-1 demonstrate the mix stretching vibrations of hydrogen bonded –OH and CH_3 groups in MAO sample while 3443, 3640 peaks for stretching vibrations of –CH_3 group in TMA solution. Relative intensity of MAO sample band at 3535 cm-1is higher than 3548 cm-1 band in TMA. [41]

2.8 Summary

The brief review of the most recent experimental and theoretical data was studied to demonstrate the structure, function and co-catalytic activity of methylaluminoxane. Main idea of current survey is to understand the structural features of MAO and successful application of metallocene catalytic system in polymer industry. Various experimental techniques i.e. NMR, IR, UV-VIS, diffusion reflection mode (DRIFT), X-ray photoelectron (XPS) spectroscopy, X-rays, SEM and inductively coupled plasma-optical microscopic were employed to evolve the structure and activation mechanism of MAO to olefin polymerization. Anyhow none of the techniques works ideally. Nano-tubular and cage structures composed of tri- and tetra-coordinated aluminum atoms were purposed by the most researchers. Experimental results suggest the TMA is a key component of MAO which has ability to control the MAO structural stability and co-catalytic activity. However, contradiction exists regarding equilibrium structure of TMA and MAO. Actual structure of MAO is still a mystery which could be finding out by applying fast and accurate computational approach in conjunction with the experimental techniques.

3 Experimental Part

3.1 Introduction

Present computational work was devoted to investigate the affinity of neutral methyl aluminoxane (MAO) to form chloride/methyl anions relative to chloride/methyl trimethylaluminum. Lower negative electronic energies ΔE_X^- of chloride/methyl aluminoxane anions than chloride/methyl trimethylaluminum anion are associated with higher affinities. Different structural motifs of anionic aluminoxane were also investigated which act as a potential co-catalyst for olefin polymerization. Theoretical results are further evaluated by electrostatic potential surfaces (ESP). Chloride/methyl MAO anions with delocalized negative charge are relatively more important than the localized ones. Uniform charge distribution over the surface can be associated with higher stability of anionic aluminoxane.

Optimized structures of MAO are classified into five groups based on degree of oligomerization. Extent of degree of oligomerization is described in term of number of oxygen and TMA molecules, denoted by n and m respectively. Active sites of MAO are identified by docking aluminum atoms with chloride/methyl anions. Further, stabilities of neutral MAO and anionic MAO structures are discussed in term of ΔE.

Research work was carried out to explore the ligand affinity as well as co-catalytic activity of MAO to metallocene pre-catalyst activation for olefin polymerization. Systematic approach was applied to first products of TMA hydrolysis to find the following objectives;

- To evaluate the feasibility of the activation step efficiently as a function of the MAO structure in terms of ligand affinities which is directly associated to the co-catalytic activity of MAO to metallocene pre-catalyst.
- Systematic study of of a wide variety of different MAOs produced by hydrolysis of TMA up to (n,m=5,4)
- Analysis of the affinities of Al-sites to find out the co-catalytically potentially active sites leading to formation of metallocene cationic centre.
- Proposals of how the chemical environment of the Al-sites should be modified to maximize the co-catalytic ability
- Evaluation of MAO counter anions stabilities by electrostatic potential maps
- Development of DFT methods could be employed in further activation studies of pre-catalyst which have capability to reproduce MP2 results

3.2 Methods and Models

3.2.1 Choice of Models

It is well known that the real structure of MAO is still a mystery. This concept leads to systematic study for MAO models of different composition and geometry. MAO oligomers are classified into five different groups with respect to number of oxygen atoms (n) where n determines the extent of degree of oligomerization. Chemical composition of MAOs were varied systematically by changing number of oxygen and TMA molecules up to (n,m=5,4).

3.2.2 Computational Details

Geometry optimization of MAO models were performed at RI-MP2/def-TZVP [55], [56] level by using TURBOMOLE V6,2 [57] program. Single point energies and electrostatic potential map calculations were done by Gaussian 0,9 [58] while results were visualized by GaussView 5.0.

3.3 MAO Anions

3.3.1 TMA and TMA Dimer

Optimized structures of neutral TMA, TMA dimer and their respective chloride/methyl anions are presented in Table 1. ΔE of TMA anions is set to zero to have a reference value for all other MAO anions. Here we are only treated the relative affinities of MAO anions rather than absolute values. Relative affinity tells how much better each Al site is in comparison to poor Al site in TMA molecule. Relative anionic affinity ΔE_X^{-1} of any MAO anion is calculated by the following formula;
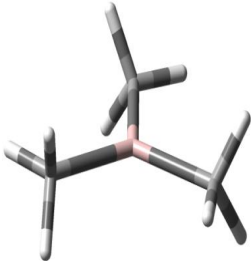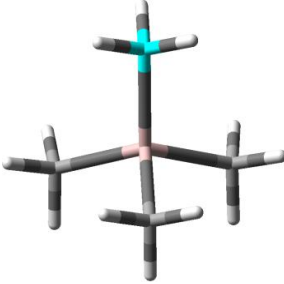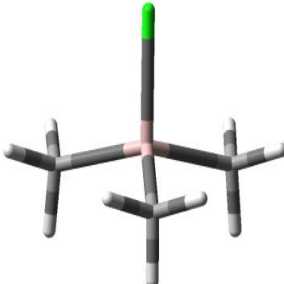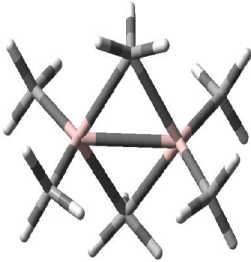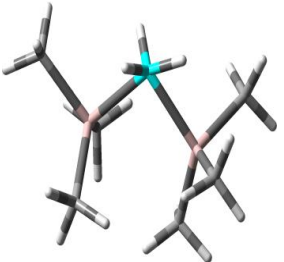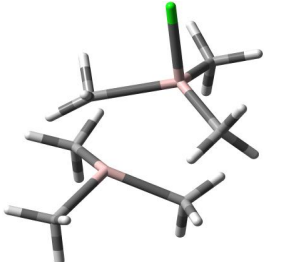
$$[\Delta E]_X^{-1} = [\Delta E]_{MAO\ anion} - [\Delta E]_{Reference\ TMA\ anion}$$

TMA molecule is planar structure in which aluminum atom is bonded to three methyl groups. Chloride/methyl ligands are attached to aluminum atom in perpendicular direction of TMA molecule plane. Planar structure of TMA transform into tetrahedral structure due to ligand attachment. TMA dimer has a bridge structure with two equivalent tetra-coordinated Al atoms. Optimized structures of TMA and TMA dimer anions are illustrated in Table 1.

TMA molecule is planar structure in which aluminum atom is bonded to three methyl groups. Chloride/methyl ligands are attached to aluminum atom in perpendicular direction of TMA molecule plane. Planar structure of TMA transform into tetrahedral structure due to ligand

attachment. TMA dimer has a bridge structure with two equivalent tetra-coordinated Al atoms. Optimized structures of TMA and TMA dimer anions are illustrated in Table 1.

Table 1. $[\triangle E]_{X^{-1}}$ (kJ/mol) of TMA and TMA dimer anions

Fig.	Neutral MAO	Me- MAO ΔE_{Me^-}	Cl- MAO ΔE_{Cl^-}
a	AlMe$_3$	0,0	0,0
b	Al$_2$Me$_6$	9,3	24,4

ΔE_{Me^-} *Relative electronic affinity of MAO for methyl ligand*

ΔE_{Cl^-} *Relative electronic affinity of MAO for chloride ligand*

TMA dimer anions have 9,3 and 24,4 kJ/mol higher energies than TMA anion. The higher energies are directly related to the lower affinities of TMA dimer for ligands. Poor affinity of TMA dimer for ligands in comparison to reference TMA can be attributed to the splitting of the structure into two parts which is not feasible for ligand abstraction reaction. The AlMe$_3$ has electron deficient three coordinated Al centre, while aluminums in Al$_2$Me$_6$ are both coordinatively saturated. The approaching ligand dissociates the TMA dimer into two TMA parts on expense of energy (Fig. 1b). One part of TMA dimer with chloride has tetrahedral structure similar to TMA anion while other resembles to the neutral TMA. On the other hand, methyl ligand formed a bridged structure between the aluminum atoms. Al$_2$Me$_6$ has shown higher affinity for methyl ligand than chloride because both Al atoms participate to abstract the methyl ligand rather than single Al atom.

3.3.2 MAO oligmers (n=1, m=1 to 3)

Optimized structures of neutral MAO and respective chloride/methyl MAO anions up to (n,m)=(1,3) with their affinity ΔE_X^- values are given in Table 2. Al_2Me_4O has two similar tri-coordinated aluminum atoms with planar geometry. Each aluminum atom is substituted by two methyl groups and one oxygen atom which join the both of aluminum atoms. Planar structure of Al_2Me_4O tends to twist in V shape with a rotation of both methyl groups with the ligand approach (Fig. 2a). Al_3Me_7O contains two types of active sites, one is tetra-coordinated and other one is tri-coordinated aluminum atom (Fig. 2b). Tetra-coordinated aluminum atoms are present in the form of ring structure in which methyl substituent form a bridge structure between aluminum atoms. No structural changes are observed as the chloride/methyl ligand approaches to tri-coordinated aluminum atom. However, when chloride/methyl ligand bonded to one of tetra-coordinated aluminum atom, it causes to transfer a penta valent methyl group to other tetra-coordinated aluminum atom and chloride/methyl formed a bridge between two tri-coordinated aluminum atoms.

$Al_4Me_{10}O$ has two isomers as denoted by 2c and 2e. 2c has four tetra-coordinated aluminum atoms forming two square faces. All the aluminum sites are chemically equivalent and joined together by single oxygen atom. 2e also composed of four non-equivalent tetra-coordinated aluminum atoms which differ on the base of chemical environment.
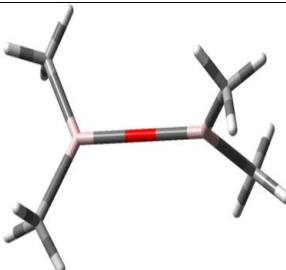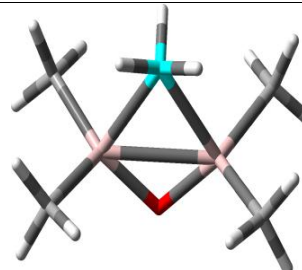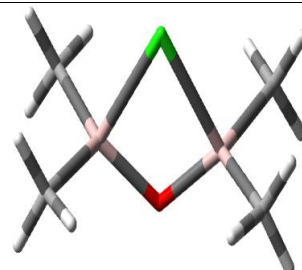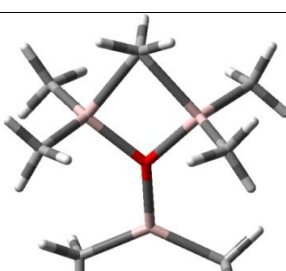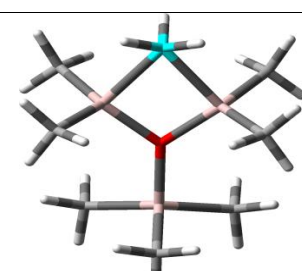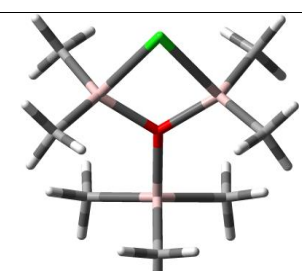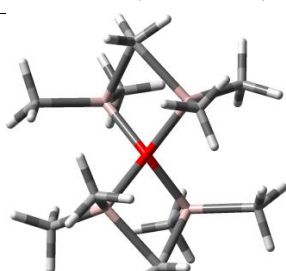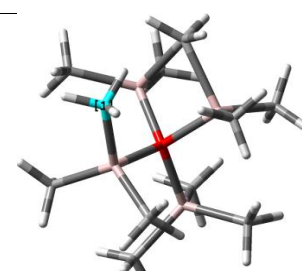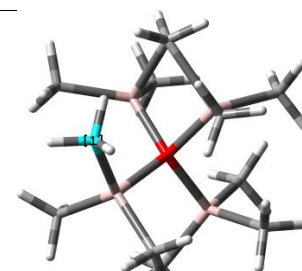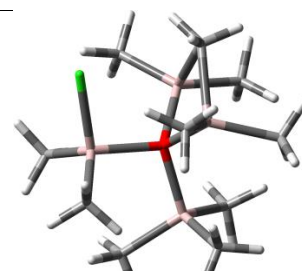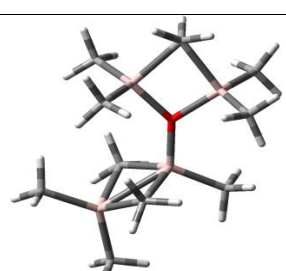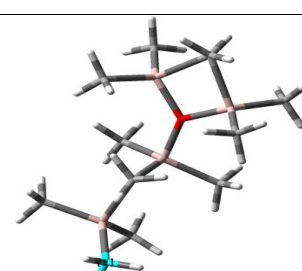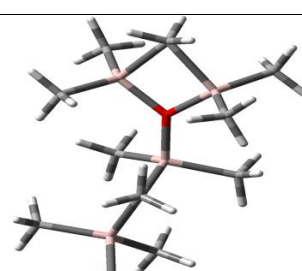
Ligand attack involves the ring opening similar to Al_2Me_6 which can be again associated the lower affinity. 2e has a less compact structure as compare to 2d and has low structural strain. This factor contributes to the higher affinity of 2e than 2d. Lower affinity of 2e than 2b can be referred to the neighboring atoms in which Al-Ligand site is not directly bonded to oxygen atom.

Chloride/methyl ligands can possibly approach to tetra-coordinated aluminum atoms bonded with tri-coordinated oxygen atoms in 2e to form bridged structure similar to 2b but there is no tri-coordinated Al atom present at β-position to accept the shifting methyl group to stabilize the anion. Bonding nature of oxygen atom also significantly contributes to the structural stability and ligand affinity of MAO. The higher affinity of 2b than 2a is associated to bridged methyl group and tri-coordinated oxygen atom connected with tetra-coordinated aluminum site.

It is observed that MAOs (n = 1) capable to form a bridge structure with chloride/methyl ligands have shown lower affinity for methyl ligands. The relative stabilities of bridged MAO-Cl$^-$ ranges from -6 to -21,9 kJ/mol which is about -1,7 kJ/mol less than non-bridged MAO-Me$^-$. Relative affinity of bridged structures is also increased with increase of m while inverse is true for non-bridged structures.

According to theoretical data it is concluded that MAO-Cl$^-$ anions have higher affinity in bridged structures which is formed between two tetra-coordinated aluminums bonded with tri-coordinated oxygen. MAO-Me$^-$ anions are found to form more stable open chain structures rather than ring structures. In a nut shell, on the base of neutral MAO structures; it is concluded that tetra-coordinated Al atoms forming a methyl bridged structures possess higher affinities than tri-coordinated Al atoms. MAOs wich are not fully saturated with TMA possess high

Table 2. MAO Structures (n=1, m=1 to 3) and [⊿E]$_X$- (kJ/mol)

Fig.	Neutral MAO	Me- MAO ΔE$_{Me^-}$	Cl- MAO ΔE$_{Cl^-}$
a	 Al$_2$Me$_4$O *(n=1, m=1)*	 -14,3	 -36,2
b	 Al$_3$Me$_7$O *(n=1, m=2)*	 -80,9	 -86,5
c	 Al$_4$Me$_{10}$O_1 *(n=1, m=3)*	 -42,8	 -25,9
d		 -45,8	 -20,0
e	 Al$_4$Me$_{10}$O_2 *(n=1, m=3)*	 -54,8	 -31,2

ΔE$_{Me^-}$/ΔE$_{Cl^-}$ *Relative electronic affinity of MAO for methyl chloride ligands respectively*

affinity according to 2b and 2c. Not only the composition (n,m) but structural alternation as well affects the ligand affinity.

3.3.3 MAO oligmers (n=2 m=2 to 4)
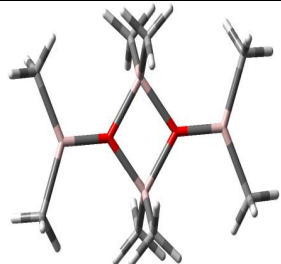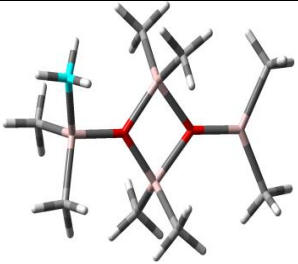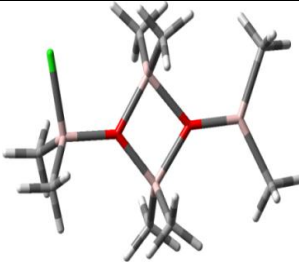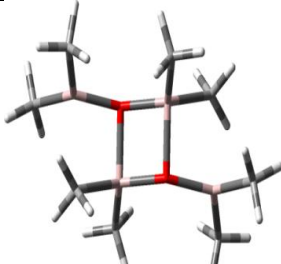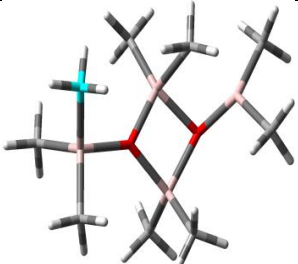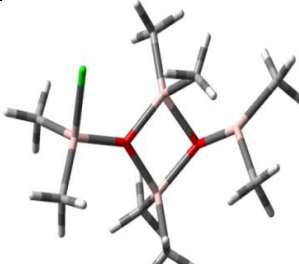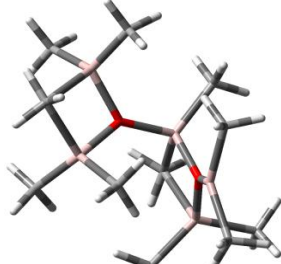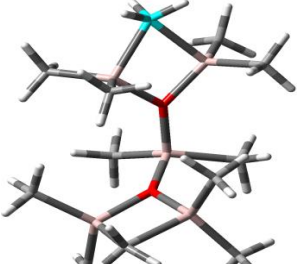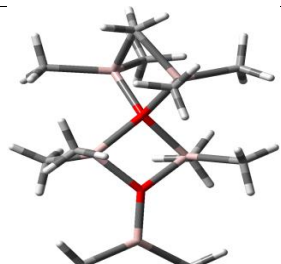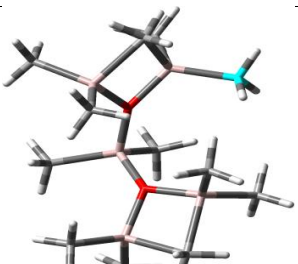
The optimized structures of neutral MAO and respective MAO anions with n=2 with their affinities ΔE_X^- are presented in Table 3. $Al_4Me_8O_2$ has two structural isomers. Both isomers composed of four member ring along w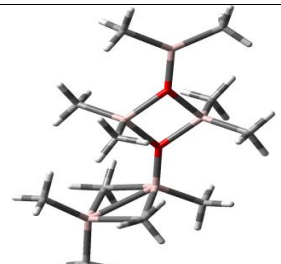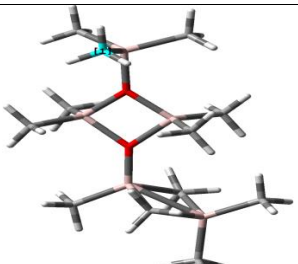ith two types of aluminum sites (Fig. 3a and 3b). In these structures, square ring is formed by joining two tetra-coordinated Al and two tri-coordinated oxygen atoms. Tri-coordinated Al atoms substituted on square rings have shown higher affinities for ligands.
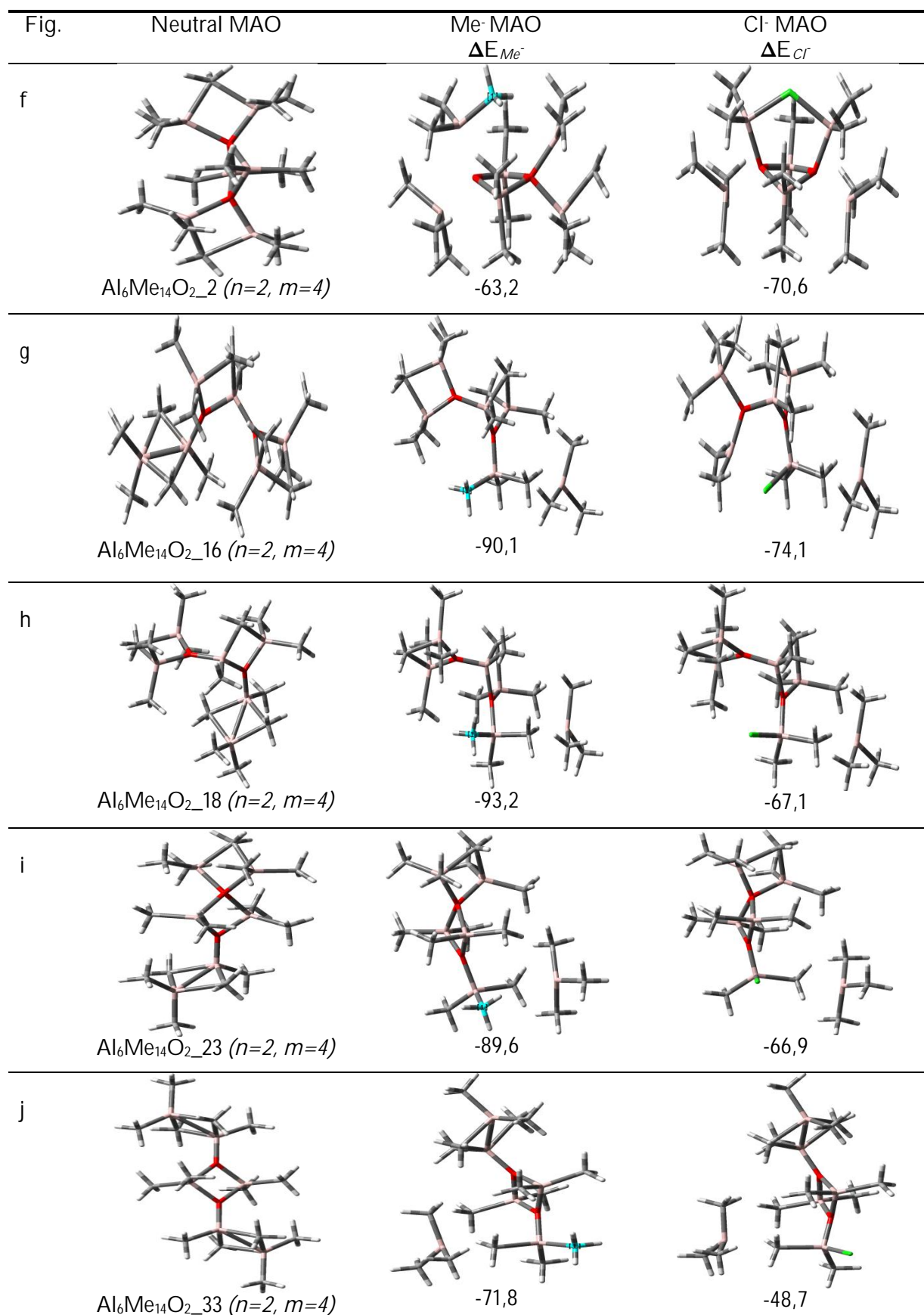
$Al_5Me_{11}O_2$ has three isomers which are denoted by 3c, 3d and 3e. The basic structural unit of 3c resembles with 2b and similarly penta-valent methyl group is transferred to adjacent tri-coordinated Al atom. Theoretical calculations reveal that tetra-coordinated aluminum atom situated close to tri-coordinated aluminum atom possess higher affinity for chloride/methyl anions. 3d and 3e are relatively planar structures with a square ring which is similar to 3a. The basic structural unit of 3d and 3e structures is also composed of one square ring which is composed of two tri-coordinated oxygen and tetra-coordinated Al atoms. This square ring has both tri-coordinated and tetra-coordinated Al atoms. Here again, tetra-coordinated Al atoms has shown higher affinities for chloride/methyl ligands. Chloride/methyl ligands cause to transform the 3d structure into 3c. Chloride and methyl MAO anions of 3c have -42,7 and -5,9 kJ/mol lower energies which is associated to higher affinities than 3d. This lower affinity of 3d is due formation of non-bridged structure.

$Al_6Me_{14}O_2$ has six isomeric forms with tetra-coordinated aluminum atoms. All isomers contain three four member rings which are either in the form of methyl bridged rings or simple four member rings. 3g, 3h and 4i isomers show higher affinities for chloride/methyl ligands than other isomers. These three non planarisomers contain bridge structures which are formed by two tetra-coordinated aluminum atoms and two bridging methyl atoms. 3g and 3i structures are similar to 3c and 3d. Bond formation of chloride/methyl ligands with tetra-coordinated aluminum atoms cause to form the TMA molecule similar to Al_2Me_6. Lower affinity of $Al_6Me_{14}O_2$ isomers is associated to the dissociation of the structures.

In general MAOs with n=2 has two types of structural motifs. First are those which contain a square ring formed by two tri-coordinated oxygen and two tetra-coordinated Al atoms. The examples of these kind of structures are 3a, 3b, 3d, 3e, 3f, 3I and 3j. The affinity of these structures decreases with the increase of m up to 4. Tri-coordinated Al atoms substituted on these rings possesses higher affinities than tetra-coordinated Al atoms. The other key structural component is composed of bridged methyl group as presented in Fig. 3c, 3g, 3h. These structures also resembles with 2b with active tetra-coordinated Al atom. The affinity of such tetra-coordinated Al atom is increased with the increase of n and m values up to (2,3) starting from (1,2) however decrease in affinity is observed with (2,4) due to dissociation of the structure.

Table 3. MAO Structures (n=2, m=2 to 4) and $[\Delta E]_{X^-}$ (kJ/mol)

Fig.	Neutral MAO	Me⁻ MAO ΔE_{Me^-}	Cl⁻ MAO ΔE_{Cl^-}
a	$Al_4Me_8O_2\_7$ *(n=2, m=2)*	-70,5	-59,0
b	$Al_4Me_8O_2\_11$ *(n=2, m=2)*	-99,9	-94,7
c	$Al_5Me_{11}O_2\_11$ *(n=2, m=3)*	-116,6	-116,1
d	$Al_5Me_{11}O_2\_20$ *(n=2, m=3)*	-110,7	-73,4
e	$Al_5Me_{11}O_2\_24$ *(n=2, m=3)*	-71,9	-57,8

Fig.	Neutral MAO	Me⁻ MAO ΔE_{Me^-}	Cl⁻ MAO ΔE_{Cl^-}
f	Al₆Me₁₄O₂_2 (n=2, m=4)	-63,2	-70,6
g	Al₆Me₁₄O₂_16 (n=2, m=4)	-90,1	-74,1
h	Al₆Me₁₄O₂_18 (n=2, m=4)	-93,2	-67,1
i	Al₆Me₁₄O₂_23 (n=2, m=4)	-89,6	-66,9
j	Al₆Me₁₄O₂_33 (n=2, m=4)	-71,8	-48,7

ΔE_{Me^-}/ΔE_{Cl^-} *Relative electronic affinity of MAO for methyl chloride ligands respectively*

Structural analysis of MAO (m=2, 3, 4) predict that bent structures which are capable of forming bridge structures, have shown higher affinities. Calculations suggest that 3c has higher co-catalytic activity than 3b and 3h. Tetra-coordinated Al atoms containing bridged methyl and tri-coordinated oxygen possess higher affinity which is in agreement with the first degree of polymerization. It is also observed that MAOs which are not fully saturated with TMA have shown higher affinities. Methyl anions are more stable than chloride anions. Methyl ligands prefer to form non-bridged structures owing to steric strain.

Structural isomerism contributes more in second degree of polymerization than first one. Higher composition (n,m) of MAO gives rise to more isomer structures. The highest isomeric effect on affinities was observed in $Al_5Me_{11}O_2$ molecule which is $\approx$ 51 kJ/mol higher than 1st degree of polymerization case ($\approx$ 10 kJ/mol). It can be concluded that the affinities of MAO increases with increase of n,m values from (1,1) to (2,3).
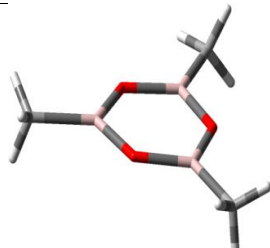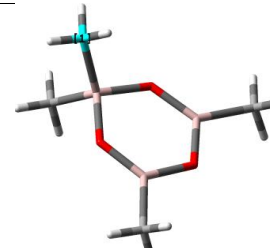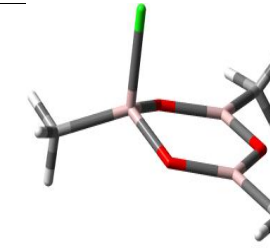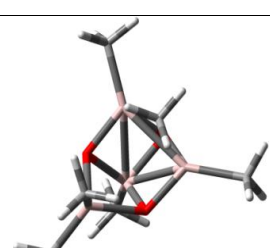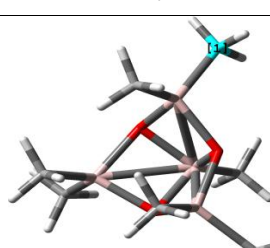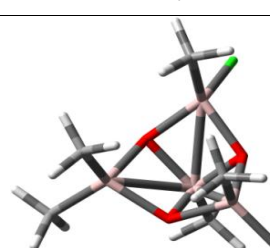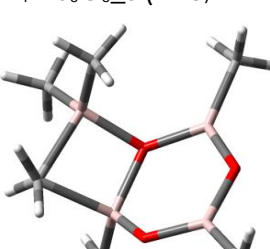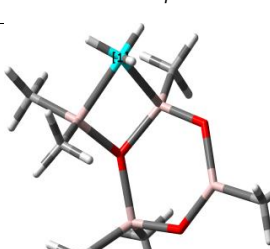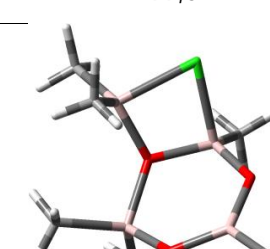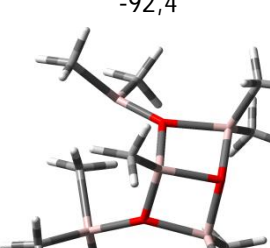
3.3.4 MAO oligmers (n=3 m=0 to 3)

Optimized structures of neutral MAOs (n,m=3,3) and respective chloride/methyl anions are illustrated in Table 4. In general, five types of structural motifs are found within third degree of polymerization. Hexagonal and diffused square rings have shown higher affinities (Fig. 4f, 4g) than other models. Both of these Hexagonal and diffused square rings are formed with n=3 rather than previous cases. Ligand affinity values are increased linearly with increase of m from 0 to 3 for both structures.

$Al_3Me_3O_3$ is a TMA deficient hexagonal ring which is composed of three equivalent tri-coordinated aluminum atoms and three di-valent oxygen atoms. Same hexagonal structural feature is also present in $Al_4Me_6O_3$, $Al_5Me_9O_3$ and $Al_6Me_{12}O_3$ models. 4c and 4e hexagonal structures have two different active sites. Tri-coordinated Al of the hexagonal ring is similar to 4a while other one is substituted tetra-coordinated Al atom. Tri-coordinated Al atoms of ring which have capacity to form bridged structure with ligands show the higher affinity in comparison to substituented Al atoms. However substituted tri-coordinated aluminum atom on hexagonal rings has shown higher affinity in case of $Al_6Me_{12}O_3$ molecule (4g). This observation suggests that tri-coordinated aluminum atom of hexagonal rings has higher aff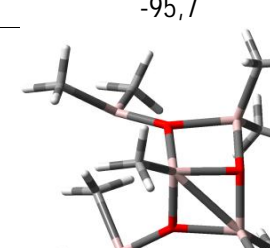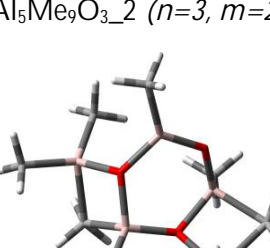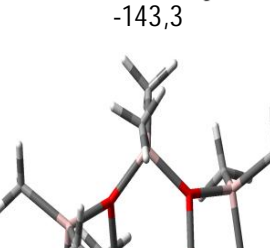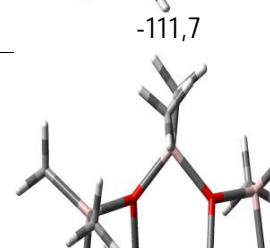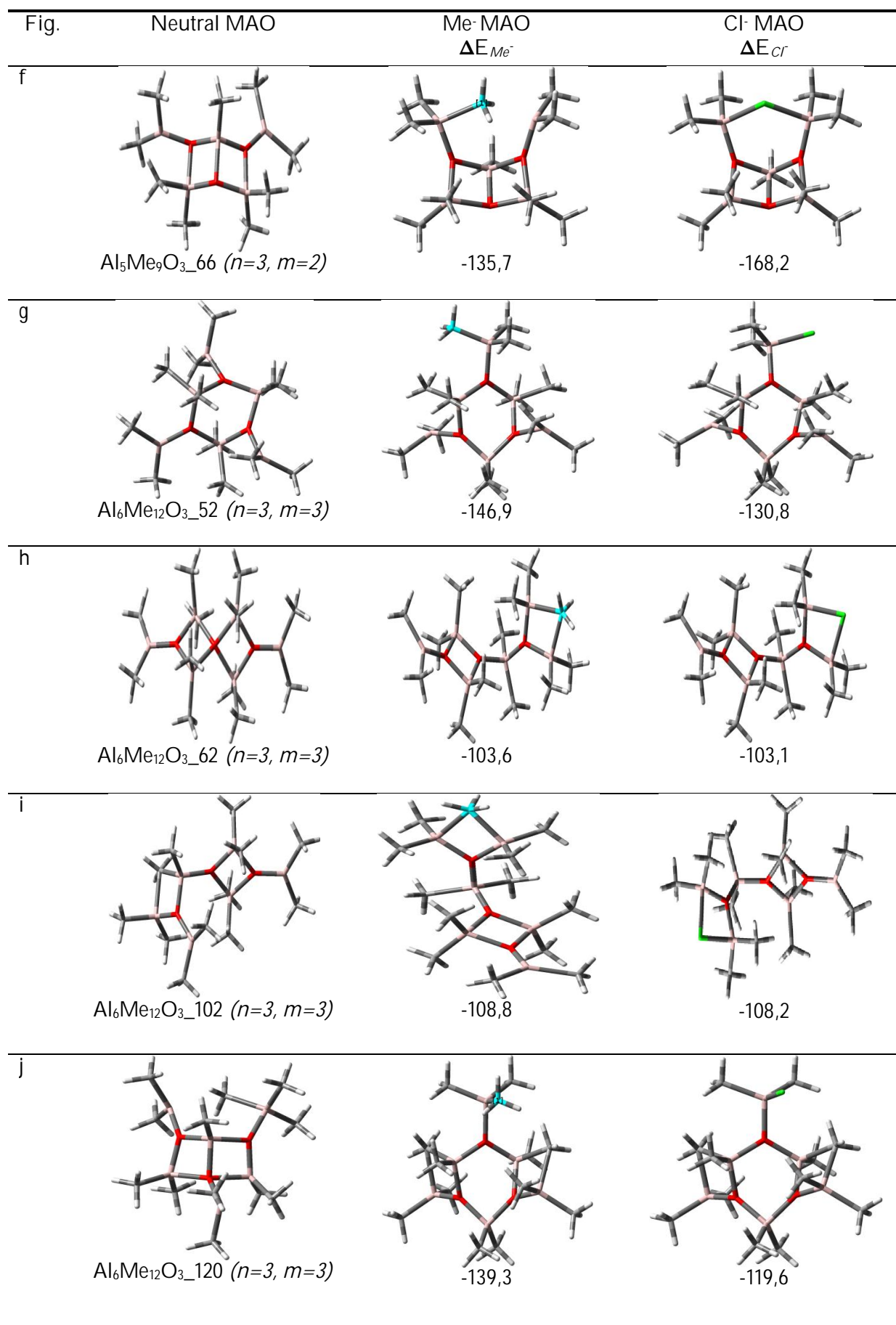inity than substituted aluminum atoms in unsaturated MAOs (n>m) where n is 3. This effect is generated due to increase in TMA contents. With the increase of m values, tri-coordinated aluminum atoms of hexagonal ring are going to saturate and finally all three tri-coordinated aluminum atoms of hexagonal ring are fully saturated with TMA at m=3.

Diffused square rings also formed in present case as shown in Figure 4b, 4d, 4f, 4j. 4b and 4d contains three and four type tetra-coordinated aluminum atoms respectively. However, methyl bridged tetra-coordinated aluminum atoms have higher affinity than other aluminum sites. Methyl bridge structure is cleaved with the ligands attack at the expense of energy which is similar to Al2Me6 case. 4f and 4j structures have tri and tetra-coordinated aluminum active sites. Distinct feature of diffused square ring structure is observed with m=3. TMA saturated square

Table 4. MAO Structures (n=3, m=0 to 3) and [⊿E]$_{X^-}$ (kJ/mol)

Fig.	Neutral MAO	Me⁻ MAO ΔE$_{Me^-}$	Cl⁻ MAO ΔE$_{Cl^-}$
a	Al$_3$Me$_3$O$_3$ *(n=3, m=0)*	-26,7	-16,9
b	Al$_4$Me$_6$O$_3$_5 *(n=3, m=1)*	-127,7	-99,5
c	Al$_4$Me$_6$O$_3$_11 *(n=3, m=1)*	-92,4	-95,7
d	Al$_5$Me$_9$O$_3$_2 *(n=3, m=2)*	-143,3	-111,7
e	Al$_5$Me$_9$O$_3$_34 *(n=3, m=2)*	-132,6	-130,2

Fig.	Neutral MAO	Me⁻ MAO ΔE_{Me^-}	Cl⁻ MAO ΔE_{Cl^-}
f	Al₅Me₉O₃_66 *(n=3, m=2)*	-135,7	-168,2
g	Al₆Me₁₂O₃_52 *(n=3, m=3)*	-146,9	-130,8
h	Al₆Me₁₂O₃_62 *(n=3, m=3)*	-103,6	-103,1
i	Al₆Me₁₂O₃_102 *(n=3, m=3)*	-108,8	-108,2
j	Al₆Me₁₂O₃_120 *(n=3, m=3)*	-139,3	-119,6

$\Delta E_{Me^-}/\Delta E_{Cl^-}$ *Relative electronic affinity of MAO for methyl chloride ligands respectively*

rings (4j) tend to rearrange into hexagonal structures in order to stabilize the MAO-ligand anion which lowers the affinity of square rings.

Ligand affinity of hexagonal structures is increased with increase of m up to (3,3). It can be concluded that higher TMA contents not only enhance the structural stability but also ligand affinity of hexagonal structures. Study of diffused square rings also shows the similar results with hexagonal MAOs. 4h and 4i represent the structures containing two square rings at consecutive and alternative positions respectively which are similar to 3c and 3f. Consecutive square rings are dissociated into alternate square ring structures upon arrival of chloride/methyl ligands. Chloride/methyl ligands bind into bridged structure form. The striking feature is observed here is the slightly increase in stability of methyl bridge structures rather than chloride bridge structures. Ligand affinity of 4h and 4i rings is reduced with the increase of n,m values.
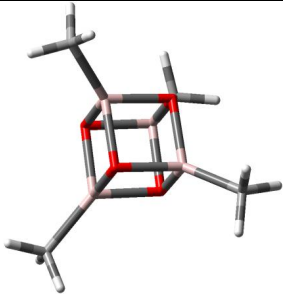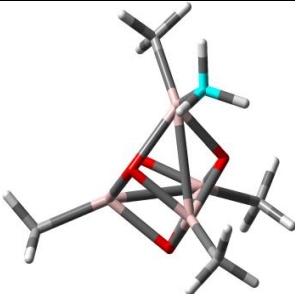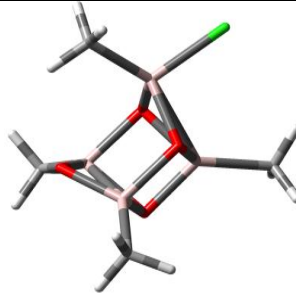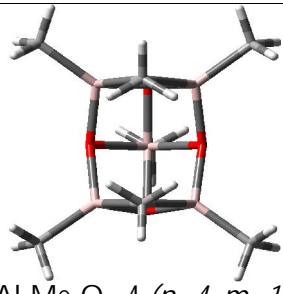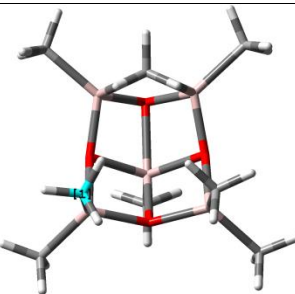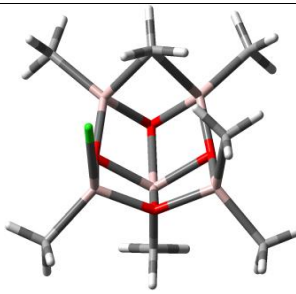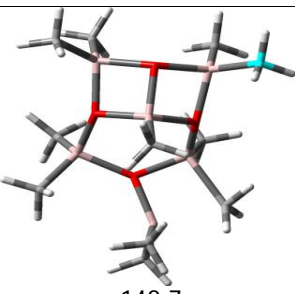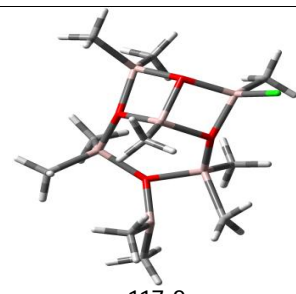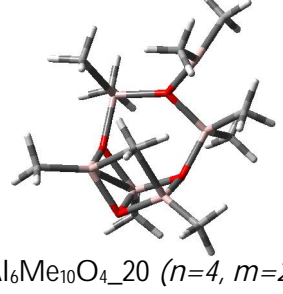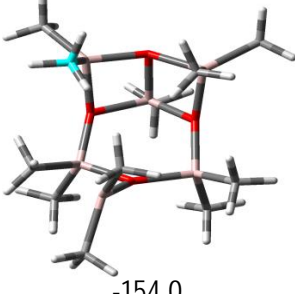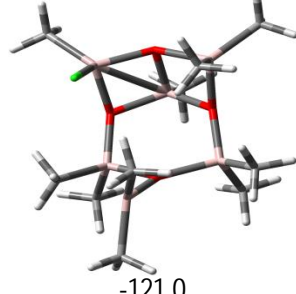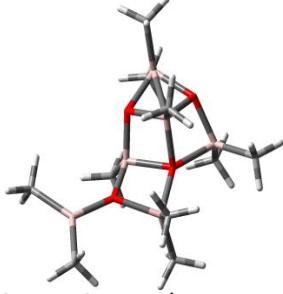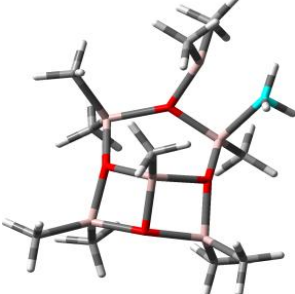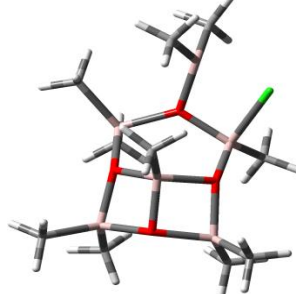
The prominent effect of composition (n, m) is observed for third degree of polymerization. It can be concluded that that the stability of neutral MAOs and their respective ligand affinity is increased with composition (n,m) which is higher than 1st and 2nd degree of polymerization. Higher TMA contents in neutral MAO correlate to higher stability and higher affinity. Fully saturated MAOs with TMA have shown lower affinities than unsaturated MAOs which reflects the unavailability of space for incoming ligand. Lower affinities for chloride ligands than methyl ligands are found in agreement with 1st and 2nd degree of polymerization. In general, tetra-coordinated aluminum active sites are found more abundant than tri-coordinated aluminum active sites. However tri-coordinated aluminum atoms in hexagonal structures are also potentially active in current case.

3.3.5 MAO oligmers (n=4 m=0 to 4)

Energetically favorable optimized structures of neutral MAO and MAO-Cl$^-$/Me$^-$ up to (n,m=4,4) are illustrated in Table 5. $Al_4Me_4O_4$ has only one cage structure isomer which is composed of four diffused square rings (Fig. 5a). There are four equivalent tetra-coordinated equivalent aluminum atoms which have lower affinity due to cage deformation. 5b and 5f is made up of curved sheet of square rings which contains tetra-coordinated Al atoms similar to 4b and 4d while 5f is ladder type structure with four square rings. Four equivalent tetra-coordinated aluminum atoms are present on the corners of the 5b and 5f structures while penta-coordinated aluminum atom is present on central position. Chloride/methyl ligands approach to the tetra-coordinated aluminum atoms containing the bridged methyl molecules.

Ladder structure (5e) contains five tetra-coordinated aluminum atoms with a different chemical surroundings where is only one tri-coordinated aluminum atom. Tetra-coordinated aluminum atom present at the interface of the cage and square ring possesses higher affinity than other aluminum sites. The structure tends to deform into hexagonal-square face structure with the ligand approach. It is also observed that tetra-coordinated aluminum atoms (Me-Al-O$_3$) have shown drastically higher affinities for methyl ligands than tri-coordinated aluminum atoms

Table 5. MAO Structures (n=4, m=0 to 4) and $[\Delta E]_{X^-}$ (kJ/mol)

Fig.	Neutral MAO	Me⁻ MAO ΔE_{Me^-}	Cl⁻ MAO ΔE_{Cl^-}
a	$Al_4Me_4O_4$ *(n=4, m=0)*	-10,2	11,8
b	$Al_5Me_7O_4\_4$ *(n=4, m=1)*	-119,5	-97,3
c	$Al_6Me_{10}O_4\_10$ *(n=4, m=2)*	-148,7	-117,2
d	$Al_6Me_{10}O_4\_20$ *(n=4, m=2)*	-154,0	-121,0
e	$Al_6Me_{10}O_4\_38$ *(n=4, m=2)*	-191,8	-187,6

Fig.	Neutral MAO	Me⁻ MAO ΔE_{Me^-}	Cl⁻ MAO ΔE_{Cl^-}
f	Al$_7$Me$_{13}$O$_4$_4 (n=4, m=3)	-117,6	-83,6
g	Al$_7$Me$_{13}$O$_4$_27 (n=4, m=3)	-113,8	-140,9
h	Al$_7$Me$_{13}$O$_4$_37 (n=4, m=3)	-129,2	-165,7
i	Al$_7$Me$_{13}$O$_4$_288 (n=4, m=3)	-125,8	-88,5
j	Al$_8$Me$_{16}$O$_4$ (n=4, m=4)	-65,4	-53,1
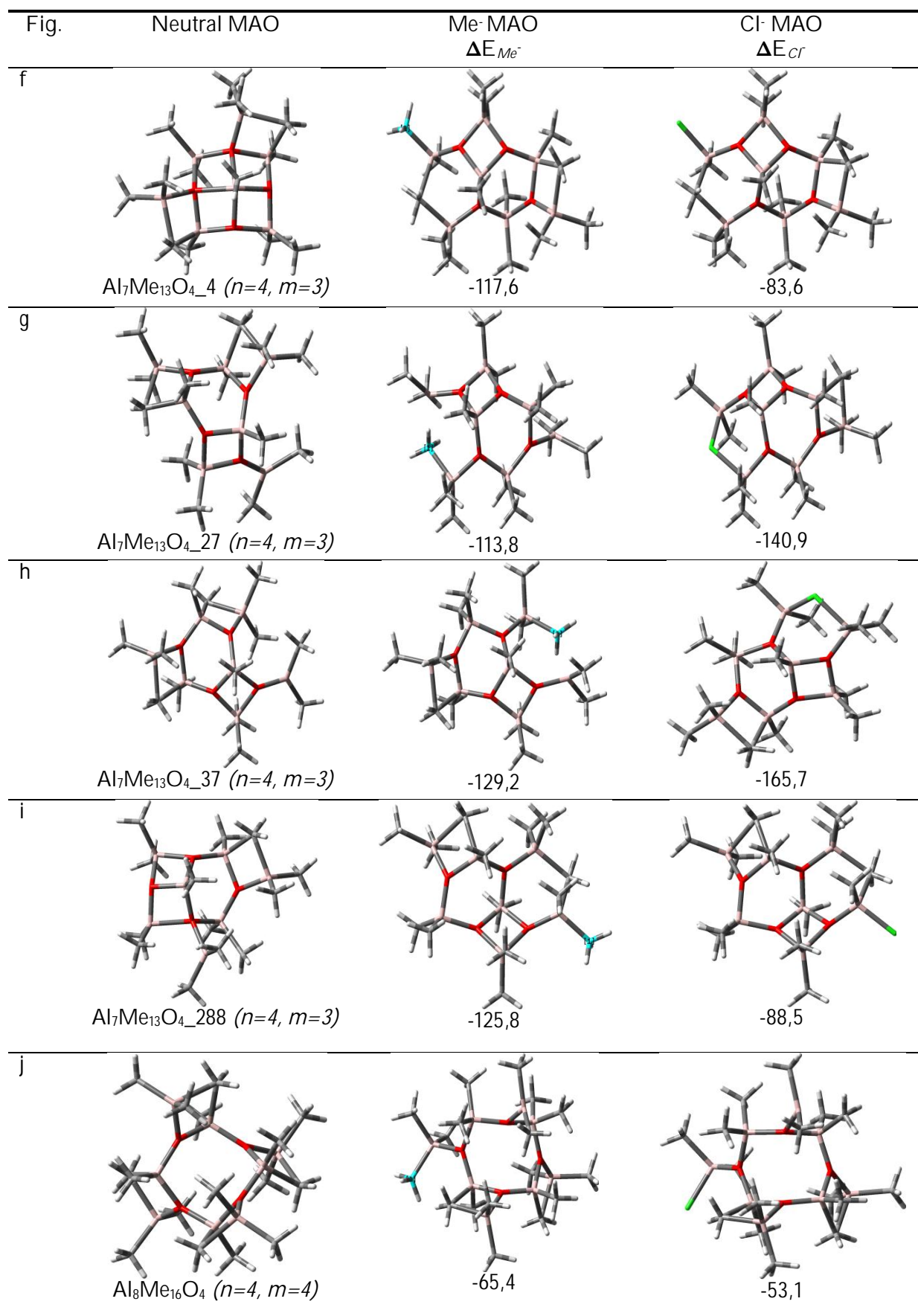
$\Delta E_{Me^-}/\Delta E_{Cl^-}$ Relative electronic affinity of MAO for methyl chloride ligands respectively

(Me$_2$-Al-O). This lower affinity is due to electron withdrawing effect of chloride ligand. Methyl ligands stabilized tetra-coordinated Al atom due to its electron donating nature while in case of chloride ligand, the Al site experienced more electronic deficiency which is associated to the lower stability of MAO-Cl$^-$anion.

Hexagonal structures are again an important feature of MAOs with n=4. Previously, we have seen that the affinity of hexagonal rings was increased with increase of m values in 3rd degree of polymerization case. However, ligand affinity of hexagonal structures is decreased by the addition of two square rings up to (4,1) but afterward it is linearly increased for higher m values. It is also observed that MAOs have lower affinities when the ligands bind to the square rings rather than hexagonal rings. Based on theoretical calculations, it can be concluded that the ligand affinity of hexagonal structures increases with increase of both n and m values in the range of (3,0) to (4,4). Saturated octagonal ring structure containing bridged methyl molecules were also studied however octagonal structure has shown lower affinities (Fig. 5j).

MAO structures with n=4 are divided into different classes to discuss the effect of n and m along with previous cases. 5a square face cage structure is only formed with n=4 but each square face resembles with 3a and 4b. Other V shape square rings with tetra-coordinated Al active atoms are also existed here. Although ligand affinity of these structures is higher than 2nd and 3rd degree of polymerization but decreases in same class with increase of m which is due to dissociation of neutral MAO structures into hexagonal-square face structures.

It is found that tetra-coordinated Al atoms possess higher affinities in present case which is in agreement with the previous calculations. 5g, 5h molecules contain tri-coordinated Al active site while the all other remaining sites are tetra-coordinated. Theoretical calculations suggest that the possible real structure of MAO consist of tetra-coordinated Al atoms which may exist in the form of square-hexagonal rings.

3.3.6 MAO oligmers (n=5 m=0 to 4)

Ligand affinities in terms of ΔE of different four types of MAOs are studied under 5th degree of polymerization. It is observed that the affinities of hexagonal rings are significantly lowered by the addition of the three square linear and cage rings (Fig. 6a, 6b and 6c) as compared to hexagonal rings containing two square face structures (Fig. 5d). Tri-coordinated Al atoms of the hexagonal ring are active sites which are similar to the 4a. Co-catalytic activity of hexagonal rings is also decreased with the increase of m. Ligand attachment to MAO molecules does not impart any significant deformation to the parent structures.

6d and 6e are composed of five member square face structures. The ligand affinity of these MAOs is also decreased with increase of m. The ligand attack causes the deformation of the parent structures into diffused hexagonal structures which are similar to 5f. Co-catalytic potential of 6d is higher than 5f. This additional stability of 6d is associated to the formation of complete hexagonal rings. 6d is the only MAO whose tetra-coordinated Al site is active as compare to other MAOs with same n=5. Ligand affinity of MAOs containing hexagonal rings is reduced as

Table 6. MAO Structures (n=5, m=0 to 4) and $[\triangle E]_{X^-}$ (kJ/mol)

Fig.	Neutral MAO	Me⁻ MAO ΔE_{Me^-}	Cl⁻ MAO ΔE_{Cl^-}
a	$Al_5Me_5O_5$ *(n=5, m=0)*	-112,8	-95,7
b	$Al_6Me_8O_5$ *(n=5, m=1)*	-90,3	-72,2
c	$Al_7Me_{11}O_5$ *(n=5, m=2)*	-100,6	-90,2
d	$Al_8Me_{14}O_5$ *(n=5, m=3)*	-163,6	-156,4
e	$Al_9Me_{17}O_5$ *(n=5, m=4)*	-115,0	-79,0

$\Delta E_{Me^-}/\Delta E_{Cl^-}$ *Relative electronic affinity of MAO for methyl chloride ligands respectively*

compared to square face structures. MAOs (n =5) has shown comparative ligand affinities to 3rd and 4th degree of polymerization while higher then 1st and 2nd degree of polymerizations.

3.4 Identification of Active Sites

Effect of different values of m with constant n and also for different n values is observed. The smallest structures of MAO (n=0-2) are less realistic models because they do not contain structural features essential for real MAO. [19], [24], [26] This aspect could be associated to random behavior of affinity for MAO-anions formation. On the other hand, MAOs with n= 3-4 are more stable models and stable anions are formed with structures n > m. MAO models with n > m indicates the TMA deficient models which have free site available for ligand abstraction. However some models are fully saturated with TMA and some are really TMA deficient that´s why we studied the all combinations of n, m.

All studied Al sites that are found in the studied MAOs are given in Figure 1. It is concluded that tetra-coordinated Al atom where methyl bridge cleavage takes place is the key component of MAO.

1) $AlC_2C_2^b$ 2) AlC_2C^bO 3) AlC_2O_2 4) $AlCO_2$ 5) AlC_2O

6) AlC_3O 7) AlC_2O_2 8) $AlCC^bO_2$ 9) $AlCC^b_2O$ 10) $AlCC^bO_2$

11) AlC^bO_2 12) $AlCO_3$
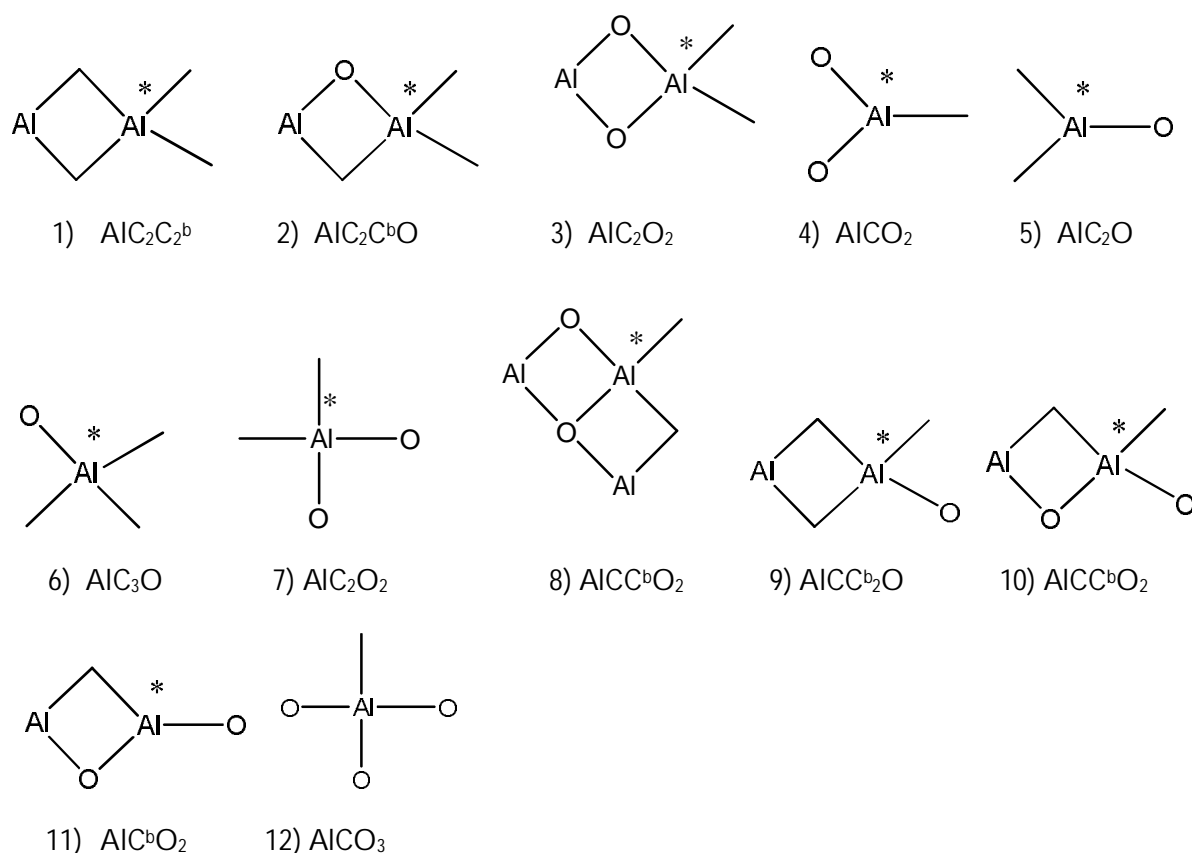
Figure 1. Reactive aluminum sites of MAO for abstraction of Cl⁻/Me⁻

Following are the structural features of active Al- sites which can improve Cl⁻/Me⁻ affinities of MAOs;

- Terminal tetra-coordinated Al- atoms capable of opening methyl bridge structures as the ligand approaches (Sites 1, 2, 8, 9, 10, and 11 in Fig.1)
- Tetra-coordinated Al atoms which are bonded to one bridge opening methyl group and one oxygen atom have higher affinities than two methyl groups (2, 8, 10 in Fig. 1)
- Tri- or tetra-coordinated Al- atoms linked to tri-coordinated oxygen atoms within non-planar structures (Sites with Al-O in Fig. 1)
- Tri-coordinated Al- atoms have higher affinity if bonded to six member ring rather than four member ring. (Site 5 in Fig.1)
- Tetra-coordinated bridged Al- atoms on diffused square rings have higher affinity than hexagonal rings (Sites 8, 10 in Fig. 1)
- Tetra-coordinated Al- atom is bonded to two tri- and one tetra-valent oxygen atoms in square rings (Site 12 in Fig.1)

Figure 2. Methyl Ligand affinities [kJ/mol] of different MAO as a function of Al-sites

Methyl ligand affinities of different MAOs as a function of Al sites are illustrated in Figure 2. It is clearly seen that most of MAO anions are formed to the following Al sites 2, 4 and 5. The anionic stability of Al site (2, 4) is growing up with increase of n and m values up to (4,3). This growth is linearly increased for MAOs with n>m. Generally, all Al sites have shown higher affinity for methyl ligands than chloride ligand. Similar 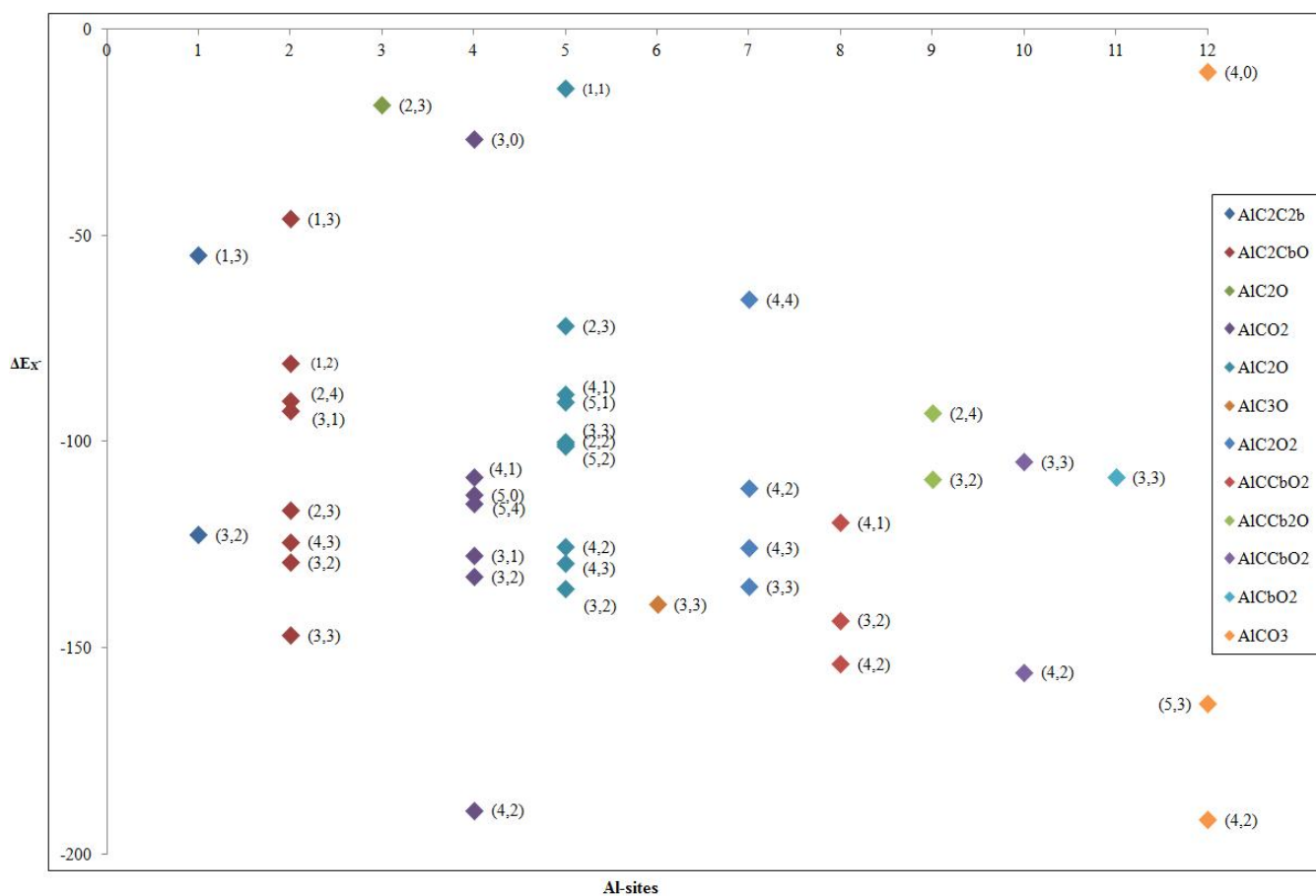effect of n and m values is observed with Al sites 8, 9, 12. Totally inverse trend of anionic stabilities is observed with site 7.

$Al_5Me_9O_3$ *(3,2)*[2] $Al_6Me_{12}O_3$ *(3,3)*[2] $Al_7Me_{13}O_4$ *(4,3)*[5] $Al_5Me_9O_3$ *(3,2)*[5]

$Al_6Me_{10}O_4$ *(4,2)*[4] $Al_6Me_{10}O_4$ *(4,2)*[8] $Al_6Me_{10}O_4$ (4,2)[4,10,12] $Al_8Me_{14}O_5$ (5,3)[12]
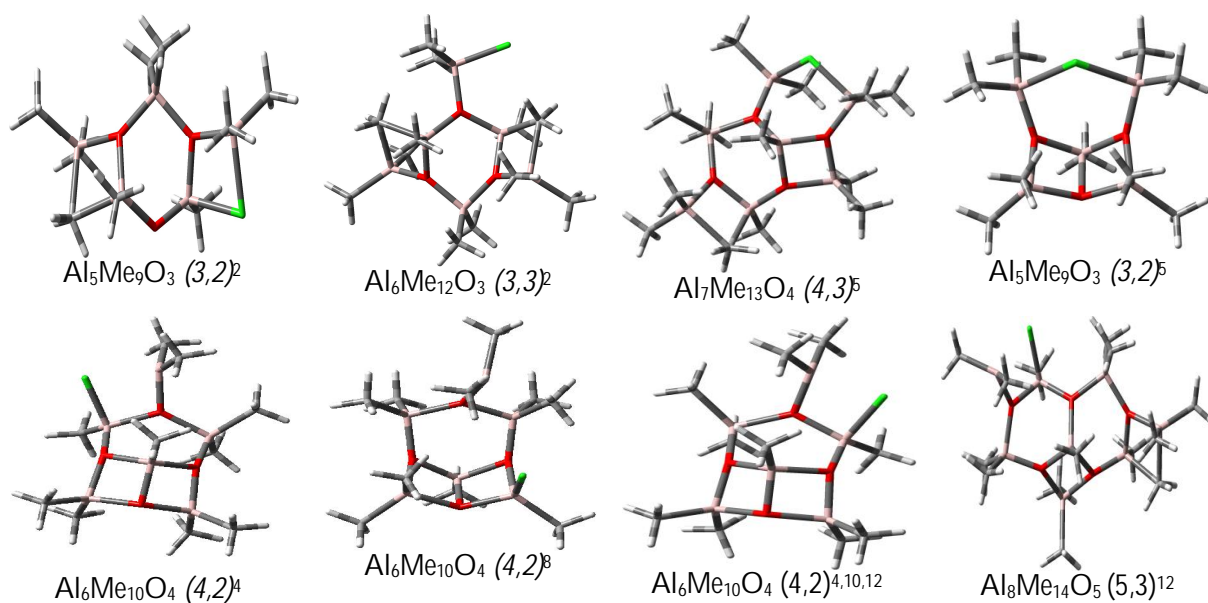
Figure 3. Most stable MAO anions Structures. Superscripts indicate the Al-sites

On the base of theoretical results it is concluded that MAOs with (3,2), (3,3), (4,2) and (4,3) are the most favorable structures which like to form MAO-anions by ligand abstraction. The most stable MAO-anions are illustrated in Figure 3. It is concluded that MAO-anions are stabilized by adopting hexagonal-square ring shapes. These justified models can employ for activation of pre-catalyst studies in future work.

Surface charge distribution describes the stability of MAO anions as compare to TMA anion. Negative charge is concentrated over chloride ligand in TMA anion as compare to other MAO anions (Figure 4). Concentrated negative charge makes TMA anion to coordinate strongly with metallocene cation thus active site is unavailable for olefin insertion. This is the reason for low yield with TMA alone. [11] On the other hand, uniform distribution of ligand charges over MAO anion surfaces makes it a better counter ion which not only stabilizes the metallocene cation but also enhance the yield of olefin polymerization.

TMA $Al_5Me_9O_3$ *(3,2)*[2] $Al_6Me_{12}O_3$ *(3,3)*[2]

$Al_7Me_{13}O_4$ *(4,3)*[5] $Al_5Me_9O_3$ *(3,2)*[5] $Al_6Me_{10}O_4$ *(4,2)*[4]

$Al_6Me_{10}O_4$ *(4,2)*[8] $Al_6Me_{10}O_4$ (4,2)[4,10,12] $Al_8Me_{14}O_5$ (5,3)[12]
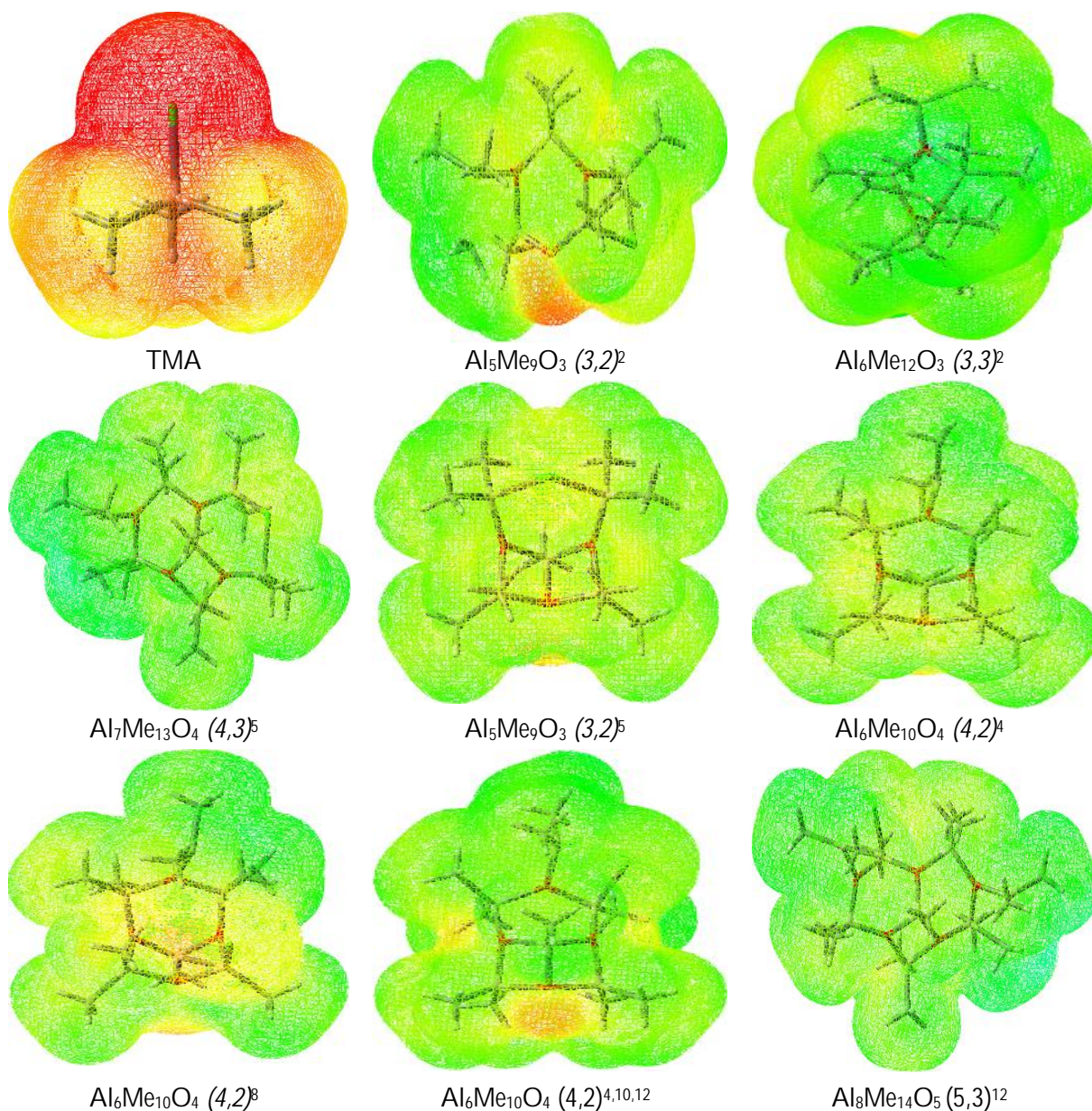
Figure 4. Surface charge densities of TMA and MAO anions

3.5 Evaluation of Computational Methods

The aim of the method evaluation was to assess the performance of different density functionals (12 functionals, SVP and TZVP basis sets) due to their computationally less intensive nature than MP2 methods and their ability to reproduce the results with same accuracy in comparison to other *ab initio* methods. Different DFT functionals were applied to investigate the reaction energies and relevant bond lengths of following reaction Cp_2ZrMe_2 + MAO (n=3,m=3) -> Cp_2ZrMe-Me-MAO which were compared with MP2/TZVP. Standard optimized Cp_2ZrMe-Me-MAO model by MP2/TZVP method is illustrated in Figure 5.

Figure 5. MP2/TZVP-calculated Cp₂ZrMe-Me-MAO reference model for DFT functionals

The results suggest M062X, WB97XD, and LSDA functionals are capable of producing reaction energies close to the MP2/TZVP-calculated energies as shown in Tables 7 and 8.

Table 7. Comparison of DFT/SVP methods with MP2/TZVP

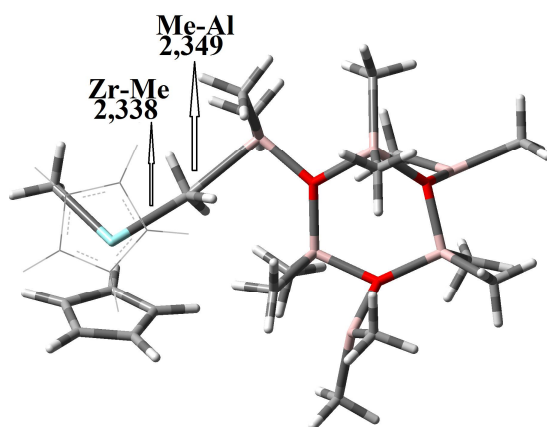|	WB97XD/SVP	M062X/SVP	LSDA/SVP	MP2/TZVP
ΔE	-56,1	-41,5	-60	-58,2
Zr-Me	2,321	2,326	2,29	2,338
Al-Me	2,38	2,367	2,271	2,349

Table 8. Comparison of DFT/TZVP methods with MP2/TZVP

	WB97XD/TZVP	M062X/TZVP	LSDA/TZVP	MP2/TZVP
ΔE	-52,4	-40,3	-51	-58,2
Zr-Me	2,329	2,337	2,301	2,338
Al-Me	2,415	2,405	2,296	2,349

LSDA method predicts considerably shorter bond lengths as compared with the MP2 results, whereas the bond lengths produced by WB97XD and M062X are in agreement with the ones produced by MP2/TZVP. WB97XD and LSDA are computationally faster methods than M062X regarding optimization time. Overall, M062X and WB97XD methods provide results in good agreement with the MP2/TZVP ones, and hence these functionals represent promising DFT methods for future studies.

3.6 Conclusions

Metallocene (pre-catalyst) along with methylaluminoxane MAO (co-catalyst) is considered as potent source for single site α olefin polymerization. Since actual structure and activation mechanism of MAO to metallocene is still unknown therefore we have identified the MAO active sites which have ability to create a stable zirconocene cationic centre. MAOs were classified into five groups based of number of oxygen and TMA molecules denoted by n and m respectively. Systematic approach was applied to study the MAO models up to n,m=5,4 composition. It is concluded that tetra-coordinated Al atom where methyl bridge cleavage takes place is the key component of MAO. The smallest structures of MAO (n=0-2) are less realistic because of their random behavior in formation of respective MAO anions while MAOs with n= 3-4 are more stable models and stable anions are formed with structures n > m. MAO models with n > m indicates the TMA deficient models which have free site available for ligand abstraction. However some models are fully saturated with TMA and some are really TMA deficient that´s why we studied the all combinations of n, m. The electrostatic potential maps indicate uniform charge distribution over MAO anions as compared to TMA anions which are associated to the higher stability to MAO anions. MAOs containing hexagonal-square rings with (3,2), (3,3), (4,2), (4,3) and (5,3) composition have shown higher thermodynamic stability as well as higher affinity for chloride/methyl ligands. These are well justified models for study of catalyst activation by MAO.

$Al_5Me_9O_3$ *(3,2)*　　$Al_6Me_{12}O_3$ *(3,3)*　　$Al_6Me_{10}O_4$ *(4,2)*　　$Al_6Me_{10}O_4$ *(4,2)*　　$Al_8Me_{14}O_5$ *(5,3)*
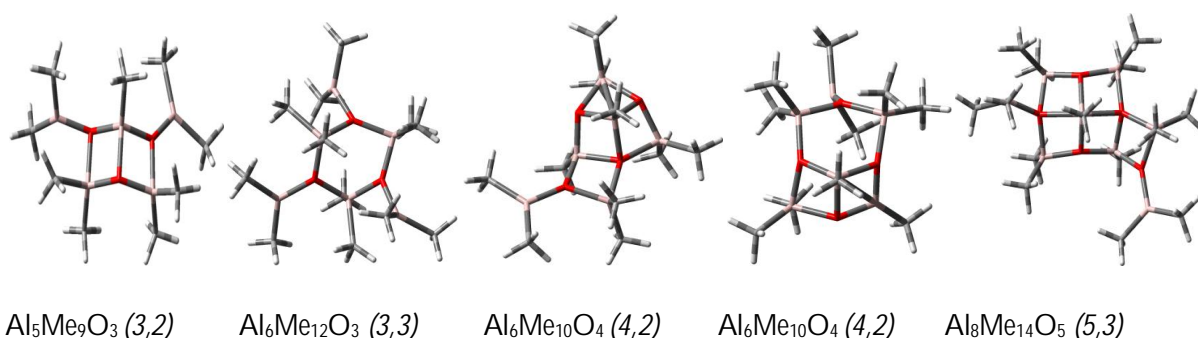
Theoretical calculations regarding DFT methods evaluation suggested the M062X and WB97XD methods provide results in good agreement with the MP2/TZVP ones, and hence these functionals represent promising DFT methods for future studies.

Acknowledgments

References

1- Ziegler, K.; Holzkamp, E.; Martin, H.; Breil, H. *J. Angew. Chem.* 1955, *67,* 541.

2- Natta, G. *J. Angew. Chem.* 1956, *68,* 393.

3- Breslow, D. S.; Newburg, N. R. *J. Am. Chem. Sot.* 1957, *79,* 5072.

4- Reddy, S. S.; Radhakrishnan, K.; Sivaram, S. *J. Prog. Ploym. Sci.* 1995, *20,* 309-367.

5- Sinn, H.; Kaminsky, W.; Vollmer, H. J.; Woldt, R.: *J. Angew. Chem. Int. Ed. Engl.* 1980, *19,* 390. b) Sinn, H.; Kaminsky, W. *J. Adv. Organomet. Chem.* 1980, *18.*

6- Resconi, L.; Cavallo, L.; Fait, A.; Piemontesi, F. *J. Chem. Rev.* 2000, *100,* 1253-1345.

7- Takagi, R.; Igata, N.; Yamamoto, K.; Kojima, S. 2010, *321,* 71-76.

8- Yang, X.; Stern, C.L.; Marks, T. *J. Angew. Chem. Int. Ed. Engl.* 1992, *31,* 1375.

9- Ewen, J.A.; Elder, M.J.: *Eur. Patent Appl.* 0 427 697, 1991.

10- Reddy, S. S.; Sivaram, S. *J. Ploym.Bul.* 1996, *36,* 165-171.

11- Tritto, I.; Boggioni, L.; Sacchi, M. C.; Dall'Occo, T. *J. Mol. Cat.* 2003, *204–205,* 305-314.

12- Zurek E.; Ziegler, T. *J. Prog. Polym. Sci.* 2004, *29,* 107-148.

13- Odian, G. G. in the book Principles of polymerization. 4th ed., Wiley & Sons, New York, 2004, p. 665-673.

14- Resconi, L.; Cavallo, L.; Fait, A.; Piemontesi, F. *J. Chem. Rev.* 2000, *100,* 1253-1345.

15- Blank, F.; Janiak, C. *J. Coord. Chem. Rev.* 2009, *253,* 827-861.

16- Brasse, M.; Cmpora, J.; Davies, M.; Teuma, E.; Palma, P.; Ivarez,E.; Sanz, E.; Reyes, M. L. *J. Adv. Synth. Catal.* 2007, *349,* 2111-2120.

17- Gladysz, J. A. *J. Chem. Rev.* 2000, 100, 1167–1168

18- Faingol´D, E. E.; Bravaya, N. *J. Polimery,* 2008, *53,* 358-363.

19- Ewen, J. A.; Jones, R.L.; Razavi, A.; Ferrara, J. *J. Am. Chem. Soc.* 1988, *110,* 6255-6256.

20- Ewen, J. A. *J. Am. Chem. Soc.* 1984, *106,* 6355-6364.

21- Kaminsky, W.; Külper, K.; Brinzinger, H. H.; Wild, F. R.W.P. *J. Angew. Chem. Int. Ed. Engl.* 1985, *24,* 507-508.

22- Piel, T. *Doc.Dis.* 2007, *74,* 58.

23- Helaja, T. in the thesis Synthesis of functionalised alkenes and their interaction with a zirconocene-methylaluminoxane catalyst system. 1999.

24- Hamielec, A. E.; Soares, J. B. P. *J. Prog. Polym. Sci.* 1996, *21,* 651-706.

25- Luhtanen, T. N. P.; Linnolahti, M.; Pakkanen, T. A. *J. Organomet. Chem.* 2002, *648,* 49–54

26- Atwood, J. L.; Hrncir, D. C.; Priester, R. D.; Rogers, R. D. *J. Organom.* 1983, *2,* 985 – 989.

27- Earley, C. W. *J. Mol. Strc. Theochem.* 2007, *805,* 101–109.

28- Zurek, E.; Woo, T. K.; Firman, T. K.; and Ziegler, T. *J. Inorg. Chem.* 2001, *40,* 361-370.

29- Mason, M. R.; Smith, J. M.; Bott, S. G.; Barron, A. R. *J. Am. Chem. Soc.* 1993, *115,* 4971.

30- Harlan, C. F.; Mason, M. R.; Barron, A. R. *J. Organom.* 1994,*13,* 2957.

31- Pasynkiewicz, S. P. *J. Organom.*1990, *9,* 429–453.

32- Sinn, H. J. *J. Macromol. Symp.* 1995, *97,* 27–52.

33- Barron, A. R. *J. Macromol. Symp.* 1995, *97,* 15–25.

34- Negureanu, L.; Hall, R. W.; Butler, L. G.; Simeral, L. A. *J. Am.Chem. Soc.* 2006, *128,* 16816–16826.

35- Zurek, E.; Woo, T. K.; Firman, T. K.; Ziegler, T. *J. Inorg. Chem.* 2001, *40,* 361–370.

36- Linnolahti, M.; Severn, J. R.; Pakkanen, T A. *J.Angew. Chem. Int. Ed.* 2008, *47,* 9279 – 9283.

37- Linnolahti, M.; Severn, J. R.; Pakkanen, T A. *J. Angew. Chem. Int. Ed.* 2006, *45,* 3331– 3334.

38- Glaser, R.; Sun, X. *J. Am. Chem. Soc.* 2011, *133,* 13323–13336.

39- Yamasaki T. *J. cat. today.* 1995, *23,* 425-429.

40- Ystenes, M.; Eilertsen, J.L.; Liu, J.; Ott, M.; Rytter, E.; Støvneng, J.A. *J. Polym. Sci. Part A: Polym. Chem.* 2000, *38,* 3106.

41- Panchenko, V.N.; Zakharov, V.A.; Danilova, I.G.; Paukshtis, E.A.; Zakharov, I.I.; Goncharov, V.G.; Suknev, A.P. *J. Mol. Cat.* 2001, *174,* 107–117.

42- Belelli, P.G.; Branda, M.M.; Castellani, N.J. *J. Mol. Cat.* 2003, *192,* 9–24.

43- Zakharov, I. I.; Zakharov, V. A. *J. Macromol. Theory Simul.* 2001, *10,* 108–116.

44- Negureanu, L.; Hall, R. W.; Butler, L. G.; Simeral, L. A. *J. Am. Chem. Soc.* 2006, *128,* 16816-16826

45- Pol, A.; Heel, J.P.C.; Meijers, R. H.A.M.; Meier, R. J.; Kranenburg, M. *J. Organom. Chem.* 2002, *651,* 80-89.

46- Bianchini, D.; Santos, J. H. Z.; Uozumi, T.; Sano. T. *J. Mol. Cat.* 2002, *185,* 223–235.

47- Zurek, E.; Ziegler, T. *J. Inorg. Chem.* 2001, *40,* 3279-3292.

48- Jan L. Eilertsen, J. L.; Rytter, E.; Ystenes, M. *J. Vib. Spec.* 2000, *24,* 257–264.

49- Smit, M.; Zheng, X.; Loos, J.; Chadwick, J. C.; Koning, C.E. *J. Pol.y Sci. Part A. Poly. Chem.* 2005, *43,* 2734–2748.

50- Giannetti, E.; Nicoletti, G.; Mazzochi, R. *J. Polym. Sci.* 1985, *23,* 2117.

51- Ueyama, N.; Araki, T.; Tani, H. *J. Znorg. Chem.* 1973, *12,* 2218.

52- Imhoff, D. W.; Simeral, L. S.; Sangokoya, S. A.; Peel, J. H. *J.Organom.* 1998, *17,* 1941-1945.

53- Giannetti, E.; Nicoletti, G.; Mazzochi, R. *J. Polym. Sci.* 1985, *23,* 2117.

54- Sugano, T.; Matsubara, K.; Fujita, T.; Takahashi, T. *J. Mol. Cat.* 1993, *82,* 93–101.

55- Weigend, F.; Häser,M.; Patzelt, H. and Ahlrichs, R.: RI-MP2: Optimized Auxiliary Basis Sets and Demonstration of Efficiency. *J. Chem. Phys.* 1998, *294,* 143.

56- Schäfer, A.; Huber, C. and Ahlrichs, R.: Fully Optimized Contracted Gaussian Basis Sets of Triple Zeta Valence Quality for Atoms Li to Kr. *J. Chem. Phys.* 1994, *100,* 5829.

57- Ahlrichs, R.; Bär, M.; Häser, M.; Horn, H. and Kölmel, C.: "Electronic structure calculations on workstation computers: the program system TURBOMOLE", *Chem. Phys.* 1989, *162,* 165–169.

58- Gaussian 09, Revision A.1, M. J. Frisch, G. W. Trucks, H. B. Schlegel, G. E. Scuseria, M. A. Robb, J. R. Cheeseman, G. Scalmani, V. Barone, B. Mennucci, G. A. Petersson, H. Nakatsuji, M. Caricato, X. Li, H. P. Hratchian, A. F. Izmaylov, J. Bloino, G. Zheng, J. L. Sonnenberg, M. Hada, M. Ehara, K. Toyota, R. Fukuda, J. Hasegawa, M. Ishida, T. Nakajima, Y. Honda, O. Kitao, H. Nakai, T. Vreven, J. A. Montgomery, Jr., J. E. Peralta,

F. Ogliaro, M. Bearpark, J. J. Heyd, E. Brothers, K. N. Kudin, V. N. Staroverov, R. Kobayashi, J. Normand, K. Raghavachari, A. Rendell, J. C. Burant, S. S. Iyengar, J. Tomasi, M. Cossi, N. Rega, J. M. Millam, M. Klene, J. E. Knox, J. B. Cross, V. Bakken, C. Adamo, J. Jaramillo, R. Gomperts, R. E. Stratmann, O. Yazyev, A. J. Austin, R. Cammi, C. Pomelli, J. W. Ochterski, R. L. Martin, K. Morokuma, V. G. Zakrzewski, G. A. Voth, P. Salvador, J. J. Dannenberg, S. Dapprich, A. D. Daniels, Ö. Farkas, J. B. Foresman, J. V. Ortiz, J. Cioslowski, and D. J. Fox, Gaussian, Inc., Wallingford CT, 2009.